



CHIMIE NOUVELLE

LA REVUE DE CONTACT DE LA SOCIÉTÉ ROYALE DE CHIMIE

39^{ème} année - novembre 2021



Homochiralité

From Pasteur's molecular dissymmetry to homochirality: a brief overview

J. GILLET

1

Electronique et Photonique moléculaire

An overview of organic light-emitting diodes: from past generations to modern light emission principles

T. CARDEYNAELS

11

Directeurs de rédaction

Bernard Mahieu
UCLouvain, Ecole de Chimie
Place Pasteur, 1
Boite L4.01.07
1348 Louvain-la-Neuve
bernard.mahieu@uclouvain.be

Benoît Champagne
UNamur,
Département de Chimie
Rue de Bruxelles, 61
5000 Namur
benoit.champagne@unamur.be

Infographisme

emmanuel@norproduction.eu

Comité de rédaction

Kristin Bartik, ULB
Nicolas Blanchard, Université de Haute-Alsace-Université de Strasbourg
Sophie Carencu, Sorbonne Université, Paris
Frédéric Castet, Université de Bordeaux
André Colas, Dow Corning
Damien Debecker, UCLouvain
Karolien De Wael (UAntwerpen)
Philippe Dubois, UMONS
Anne-Sophie Duwez (ULiège)
Gwilherm Evano, ULB
Danielle Fauque, Université de Paris Sud
Stéphane Gérard, Faculté de Pharmacie, Reims
Bernard Joris, ULiège
Sophie Laurent, UMONS
Tatjana Parac-Vogt (KULeuven)
Raphaël Robiette, UCLouvain
Cédric Samuel, École des Mines de Douai
Armand Soldera, Université de Sherbrooke
Johan Wouters, UNamur

Secrétariat

Violaine SIZAIRE
ULB
avenue Franklin Roosevelt 50, CP 160/07 1050 Bruxelles
Tel : +32 2 650 52 08 Fax : +32 2 650 51 84 - email : src@ulb.be
Fortis : BE60 2100 4208 0470

Comité directeur

Conseil de gestion

Président	L. Provins, UCB	laurent.provins@ucb.com
Vice-présidente	A.-S. Duwez, ULiège	asduwez@uliege.be
Président sortant	B. Champagne, UNamur	benoit.champagne@unamur.be
Secrétaire générale	C. Buess-Herman, ULB	cbuess@ulb.ac.be
Trésorier	P. Laurent, ULB	plaurant@ulb.ac.be
Délégué relations extérieures	P. Baekelmans, Solvay	paul.baekelmans@solvay.com

Divisions

Chimie Médicinale	L. Provins, UCB	laurent.provins@ucb.com
Jeunes Chimistes	M. Neumann, UNamur	myriam.neumann@unamur.be
Histoire et Enseignement de la Chimie	B. Van Tiggelen	vantiggelen@memosciences.be
Délégué Essenscia Wallonie	C. Moucheron, ULB	cmouche@ulb.ac.be
	T. Randoux, Certech	Thierry.Randoux@certech.be

Sections locales

Bruxelles	G. Evano, ULB	Gwilherm.Evano@ulb.be
Louvain-la-Neuve	B. Elias, UCLouvain	benjamin.elias@uclouvain.be
Mons	P. Gerbaux, UMONS	pascal.gerbaux@umons.ac.be
Liège	A. S. Duwez, ULiège	asduwez@ulg.ac.be
Namur	B. Champagne, UNamur	benoit.champagne@unamur.be

Membres protecteurs de la SRC

ALLNEX
CERTECH
DOW CORNING
EXXONMOBIL CHEMICAL
LHOIST
SOLVAY
TOTALENERGIES
UCB

Parution : trimestrielle

Avec le soutien du Fonds National de la Recherche Scientifique.
Les articles paraissant dans Chimie nouvelle sont repris dans CHEMICAL ABSTRACTS

Editeur responsable : Claudine Buess-Herman,
ULB, CP 160/07,
avenue Roosevelt 50, 1050 Bruxelles

Les articles sont soumis à un processus de reviewing.
Les annonces publicitaires sont établies sous la responsabilité des firmes.

« CHIMIE NOUVELLE » est un titre déposé

ISSN 0771-730X

Jean GILLET

Nonlinear Physical, Chemistry Unit, CP – 231,
Université libre de Bruxelles, Avenue F. D. Roosevelt 50,
1050 Bruxelles
Jean.Gillet@ulb.be



From Pasteur's molecular dissymmetry to homochirality: a brief overview

Abstract

Since the discovery of chirality in organic molecules by Pasteur in the 19th century, the emergence of homochirality in biological molecules such as DNA and proteins has puzzled generations of scientists. Although the origin of such an asymmetry is still unknown, many researchers tried to understand the mechanism behind this symmetry breaking process through experiments and theoretical approaches. This article aims at providing a brief overview of the main experimental and theoretical contributions to this research field. In addition, the author's contributions in the framework of his master thesis as well as the investigations planned in the context of his PhD thesis are presented. This article does not claim to be exhaustive and specific but rather aims at providing an introduction to this rapidly growing research field.

Key Words

Chirality, Stochasticity, Deracemization, Hydrodynamic, Numerical Simulations



Figure 1. Louis Pasteur (1822-1895), a famous French biologist and chemist. During his lifetime, he greatly contributed to the development of microbiology. He is particularly known for his discoveries on chirality as well as his pioneering work on vaccines and Pasteurization.

1. Introduction

Our aim here is to provide the reader with a brief introduction on the fascinating question of the origins of homochirality, i.e. the property of a system composed of objects that exhibit the same chirality. First, a brief introduction about the discovery of chirality and the enigma of homochirality is presented in Sections 1.1 and 1.2. Second, the main theoretical and experimental works related to the emergence of homochirality are succinctly reviewed in Section 2. The author's contribution to this research field in the framework of his master thesis is summarized in Section 3. Finally, future works and a conclusion are featured in Sections 4 and 5.

1.1. Chirality – a breakthrough discovery of chemistry

In the 19th century, Louis Pasteur highlighted one of the most interesting features in nature known today as chirality. Since then, chirality has been a central pillar of modern chemistry and is established as an essential property that every chemist and microbiologist should take into account.

Capitalizing on the works by Fresnel and Biot on polarized light, Pasteur deduced in 1842 the existence of a “molecular dissymmetry” from a cautious study of tartaric acid crystals exhibiting an optical activity [1]. In 1874, this optical activity was connected to the tetrahedral arrangement of the atoms bound to carbon by van 't Hoff and Le Bel [2, 3]. However, the term “chirality” was only introduced by the end of the 19th century by Kelvin [4]. At the time, he proposed the following definition:

“I call any geometrical figure, or group of points, “chiral”, and say that it has chirality if its image in a plane mirror, ideally realized, cannot be brought to coincide with itself.”

In other words, an object is considered chiral when it cannot be superimposed on its image in a mirror. There are a multitude of chiral objects including molecules and galaxies, not to mention our hands. When a molecule is chiral, it will

be able to exist in two different forms called enantiomers. Over time, multiple nomenclatures have been introduced to characterize chirality, causing occasionally some confusion among scientists. The original description was based on the deviation of the plane of polarization of polarized light (*d*-dextrogyre and *l*-levogyre). Another one has been proposed regarding the absolute configuration or the spatial arrangement of the compound compared to a certain reference (D/L). This later nomenclature is still commonly used by biologist to characterize sugars and amino acids. Nowadays, the most common nomenclature used by chemists is the one proposed by Cahn, Ingold and Prelog, also known as the “priority rule” or “CIP” system [5] (Rectus and Sinister).

Two enantiomers share the same chemical formula but do not have the same geometric structure. In addition, they will have different biological properties. More precisely, a cellular receptor, which is itself chiral, can discriminate between two enantiomeric molecules by interacting with the molecule of appropriate symmetry. The simplest example to understand this is to consider a pair of gloves. A right glove is suitable for a right hand, but not for a left hand.

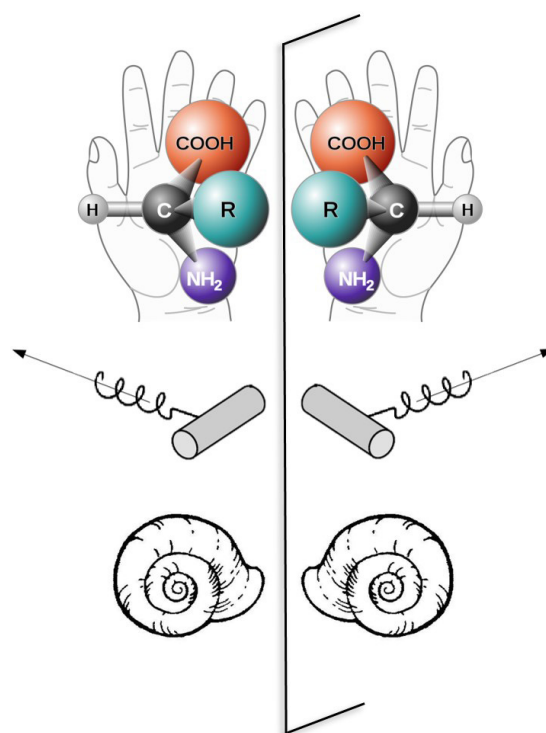


Figure 2. Illustration of various examples of chirality.

1.2. Homochirality – the new enigma of life

This preponderant role of chirality in the biological world goes back to the origins of life on earth. Indeed, nineteen of the twenty natural amino acids composing all the proteins of living things are homochiral, that is to say that they are found in a single enantiomeric form, namely, the left-handed form (Homo- from Greek “same” and -chirality derived from Kheir or “hand”). A homochiral composition is the opposite of a so-called racemic composition, in which we will find an equal distribution of the enantiomers.

Proteins are not the only macromolecules to present homochirality. Aside from its fabulous capacity of information storage, DNA exhibits the particularity to be composed almost exclusively of sugars in the right-handed form. From a chemical perspective, DNA can be considered as a polymer chain assembled from monomeric units that contain all the genetic information. Some theoretical models have been proposed to understand its growth using a stochastic approach of the underlying co-polymerisation processes. However, little attention has been paid to the chiral asymmetry and its origin.

While the focus of this research field has been initially on questions regarding the origin of homochirality in DNA and proteins, the interest has widened to numerous chemical systems. Since then, many applications have already been found such as the deracemization of organic compounds and more are expected to come in a wide variety of fields, such as polymer chemistry and self-assembled materials [6].

2. Emergence of homochirality – an asymmetric stor

Since Pasteur's works on chirality the origin of single-handedness in the biological world has remained an intriguing question. Numerous researchers tried to understand the emergence of such an asymmetry by building theoretical models. The main goal was to introduce a model presenting the amplification of a chiral state

at the expense of the mirror state, leading to a homochiral system. If research was essentially theoretical at the beginning, experimental demonstrations appeared quickly, thus motivating the understanding of the underlying mechanisms.

2.1. Theoretical models for homochirality

The construction of theoretical models exhibiting the appearance of homochiral states dates back to 1953 with the description of a minimal system containing all the necessary components by Frank [7]. Frank's original model is based on an autocatalytic production and a mutual antagonism between enantiomers.

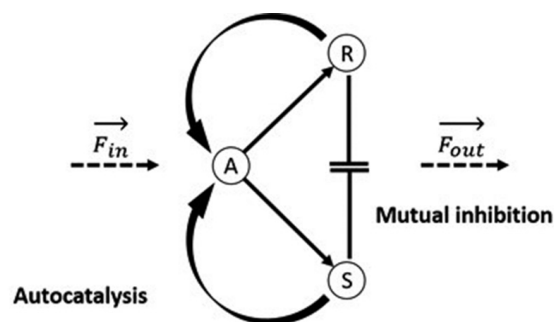


Figure 3. A relatively simple model coupling the autocatalysis with mutual antagonism between enantiomers, allowing the amplification of an enantiomeric excess until reaching a homochiral state.

This model was the first to propose a coupling between autocatalysis and symmetry breaking. By maintaining the system far from equilibrium under flow conditions, Frank's model allows a transition from a racemic state to a stable symmetry-breaking state where one or the other enantiomer is dominating beyond a certain threshold value of the matter flow parameter. Many extensions of this model have been derived, by considering, for example, a fast racemization process [8], the reversibility of reactions [9] or modifications to the mass flows [10–13].

One of the most significant modifications to Frank's model has been proposed by Kondepudi and Nelson [9]. The two main modifications were the addition of a spontaneous production of chiral products from achiral reactants and the reversibility of the production processes.

With these modifications, they demonstrated that chiral symmetry breaking may occur when the concentration of achiral reactant exceeds a certain critical concentration, resulting in the amplification of a small initial chiral bias towards homochirality.

They proposed a general equation for this symmetry breaking process which describes the evolution in time of the enantiomeric excess, α , a measure of the excess of one enantiomer compared to the other:

$$\frac{d\alpha}{dt} = -A\alpha^3 + B(\lambda - \lambda_c)\alpha + Cg$$

in which A, B, C and λ are coefficients determined by the kinetic parameters, and g is the parameter measuring the chiral bias.

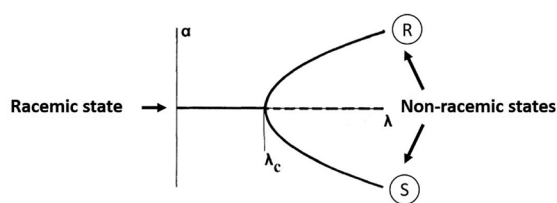


Figure 4. Chiral symmetry breaking illustrated by pitchfork-type bifurcation. Maintained out-of-equilibrium, Kondepudi's model shows a bifurcation beyond a certain critical parameter value, where the system can evolve from one racemic state to two homochiral states.

Polymers have always attracted a lot of attention due to their broad range of properties and applications. Moreover, numerous molecules essential to life are natural polymers such as DNA or proteins. It is interesting to note that the chiral properties of these biomolecules are still puzzling generations of scientist. When the possibility of chiral induction during polymerisation processes arose [14], several researchers started to study

the possibility to extend the ideas from Frank's work to polymerisation reactions. To build the bridge to polymerisation processes, Sandars proposed a variation of Frank's model including polymerisation reactions [15]. Incoming reactants provide a continuous flow of chiral monomers that can be integrated in a growing chain, which leads to heterochiral chains. The larger polymers are flushed out to maintain the system open. Later, Saito proposed a similar model including the reversibility of all the steps, except for the open flow processes [16]. In Saito's model, the reverse reactions act as a correction mechanism for the growing polymer chain.

2.2. Emergence of homochirality in experimental system

The first experimental demonstrations of the emergence of homochirality were published in the early 90s. Kondepudi and Soai reported the observation of spontaneous chiral symmetry breaking in crystallization [17] and in asymmetric autocatalysis in organic chemistry [18], respectively.

In Kondepudi's experiment, stirring a solution of NaClO_3 under crystallization conditions resulted in spontaneous chiral symmetry breaking. NaClO_3 precipitates as an enantiomeric conglomerate composed of 4 sub-units and the chirality of the resulting crystals can be detected optically. It was then assumed that the effect of stirring was central, because it would make crystallization autocatalytic and thus lead to a spontaneous chiral symmetry breaking [19]. It was suggested that a secondary nucleation process was the driving mechanism behind

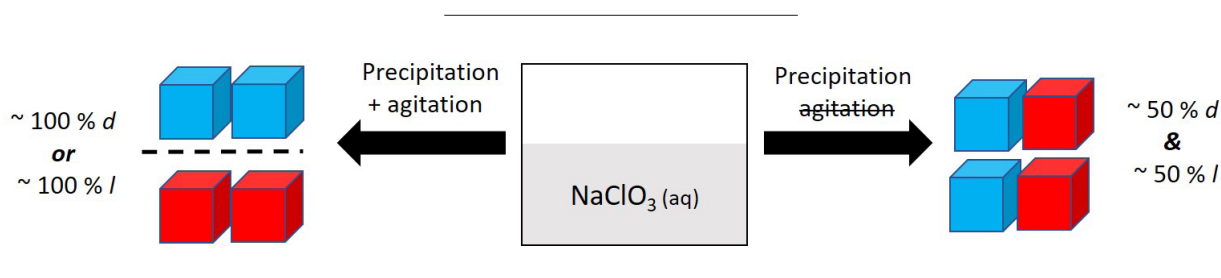


Figure 5. Illustration of Kondepudi's experimental work. When a saturated solution of Sodium Chlorate undergoes crystallisation under constant stirring, a symmetry breaking is observed in the resulting crystals. This symmetry breaking is no longer observed when the system is no longer agitated.

these results. The selection of the amplified enantiomer is arbitrary, depending on the randomly generated primary crystal.

The Soai reaction is another experimental demonstration that inspired many researchers and still attracts a lot of attention. The Soai reaction is an alkylation of aldehydes where the initial reactants A and B are achiral but the final product C is chiral. To prepare the reaction, the reactants A and B are dissolved in a solvent with a small chiral bias introduced in order to create a small imbalance. When the reaction proceeds, it manages to amplify the initial chiral bias into a non-negligible enantiomeric excess [18]. By iterating the process several times, large enantiomeric excesses close to homochirality can be obtained. One of the most impressive features of this reaction is its extreme sensitivity. Indeed, Soai managed to selectively amplify one of the enantiomers by using polarised light, chiral organic and mineral crystals but also, he demonstrated that chiral isotopic isomers, i.e. species having the same number of each isotope of each element but differing in their spatial arrangement, could act as chiral triggers of asymmetric autocatalysis [20].

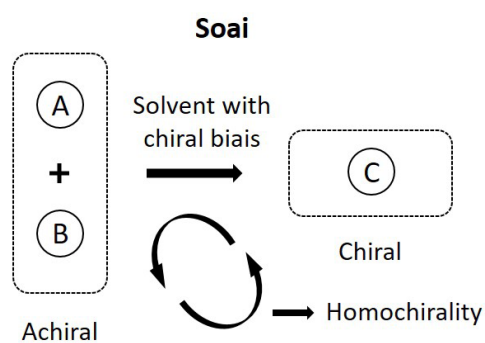


Figure 6. Starting from achiral precursors to form a chiral final product, Soai's reaction is able, after a few iterations, to amplify a small enantiomeric excess toward a homochiral composition.

Fifteen years later, Viedma was able to achieve complete deracemization of a racemic mixture of *l*- and *d*-NaClO₃ crystals using abrasive glass balls while stirring [21–23]. Based on these results, Viedma suggested that secondary nucleation is not the main reason behind deracemization. He suggested instead that glass

balls lead to grinding, which continuously crushes the growing crystals (a phenomenon often referred to as attrition). This causes a nonlinear autocatalytic-recycling process responsible for the deracemization, which can be summarized as follows: 1) Racemization in solution (not necessary for achiral molecule crystallizing as enantiomeric clusters), 2) Ostwald ripening – the growth of large crystals at the expense of smaller ones, 3) Enantioselective incorporation of chiral clusters into larger crystals, 4) Enhancement of the Ostwald ripening by attrition.

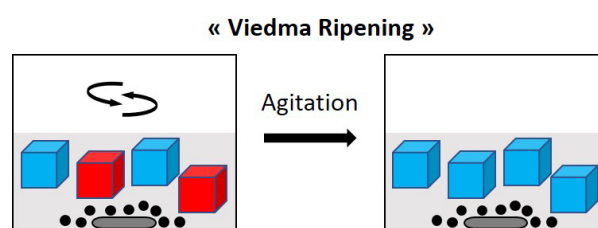


Figure 7. Illustration of the “Viedma Ripening”. Glass beads (black dots) coupled to agitation continuously crush the growing crystals leading to a complete deracemization.

This so-called “Viedma ripening”, was a big step for the implementation of a reliable resolution method for crystals and a true proof of concept for the special role played by nonlinearity in chiral symmetry breaking.

A few years later, Viedma *et al.* extended this procedure to intrinsically chiral molecules with the observation of a significant increase of the enantiomeric excess for a proteinogenic amino acid. More generally, the Viedma ripening has found many applications [23] such as the complete deracemization of pharmaceutical molecules [23–25], the total resolution of metal complexes [26, 27] or the enantioenrichment in organic chemistry reactions from chiral or achiral compounds [28–33].

To investigate the effect of grinding, Uwaha and Katsuno proposed a theoretical model which evaluates the influence of the size distribution of the chiral clusters [34]. They showed that in absence of grinding, for an appropriate size distribution, the chirality conversion can be obtained through a slow Ostwald ripening. With grinding, the initial asymmetric distribution of

chiral clusters can be rapidly amplified, leading to a homochiral state [35].

Grinding and stirring are not the only ways to achieve deracemization. Indeed, El-Hachemi *et al.* demonstrated that a temperature gradient can be sufficient to induce a strong enantiomeric excess [36]. A supersaturated solution of NaClO_3 was boiled following a distillation process where water was constantly removed. The reflux system was supposed to be determinant during the nucleation process.

In 2011, Viedma and Cintas pushed forward the effect of temperature gradients by reporting a complete deracemization from a boiled racemic mixture of *l*- and *d*- NaClO_3 crystals [37]. To obtain complete deracemization, the solution is simply heated with a hot plate at the bottom of the flask. A random distribution of the final chirality is obtained through repeated experiments, showing again the arbitrary character of the selection process. In the same study, it was also shown that the effect of the temperature gradient can be cancelled by stirring the solution.

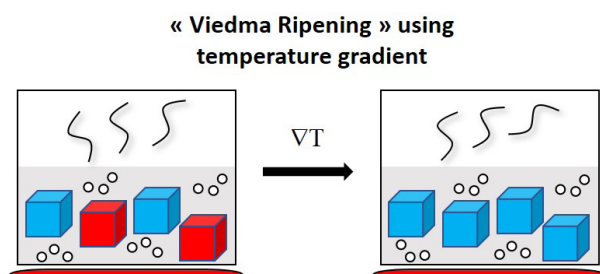


Figure 8. Illustration the “Viedma Ripening”, using a vertical temperature gradient.

Coquerel *et al.* extended this concept using heating cycles to better understand the results from Viedma and Cintas [38]. In addition to an experimental demonstration, they conducted mathematical modelling, which suggests that a difference in the crystal growth kinetics can cause chiral symmetry breaking [39]. The bubbling and the hydrodynamic flows generated by the temperature gradient were suspected to be involved in the deracemization process, but no definitive conclusion has been reached yet.

2.3. Microscopic description of homochirality

The large number of works regarding the emergence of homochirality has been succinctly reviewed in the previous paragraphs. Among these contributions, many theoretical models have been proposed to study the emergence of homochirality. Most of them rely on a so-called “macroscopic” approach. Such an approach consists in developing deterministic evolution equations that allow the prediction over time of the evolution of the collective quantities of a system such as, for example, the concentrations of different chemical species.

From a completely different perspective, “microscopic” theoretical models have been proposed to understand the growth of homochiral molecules. Unlike a macroscopic approach, a microscopic approach will try to integrate the role of processes involving individual molecules. Since these processes take place at random (they are stochastic processes), this type of approach can be qualified as probabilistic, in opposition to the determinism of macroscopic theories.

In this framework, Kondepudi and Nelson wanted to apply this probabilistic description to the chiral symmetry breaking processes. During their study on the influence of weak neutral currents on the chiral symmetry breaking process [40], they also proposed a mesoscopic approach of the transition that occurs between a racemic state and a homochiral state. Indeed, the general equation used is a Langevin equation which takes into account the stochastic character of the system’s dynamics.

More specifically, they were interested in predicting the probability with which the system evolves toward one of the two homochiral states when the value of a control parameter λ exceeds a certain threshold λ_c . To do so, they started from a Fokker-Planck equation in order to describe the evolution of the probability to have a certain chiral asymmetry α :

$$\frac{\partial}{\partial t} P(\alpha, t) = -\frac{\partial}{\partial t} [-A \alpha^2 + B (\lambda(t) - \lambda_c) \alpha + C g] P(\alpha, t) + \left(\frac{\epsilon}{2}\right) \frac{\partial^2}{\partial t^2} P(\alpha, t)$$

where $P(\alpha, t)$ is a probability density function quantifying the probability that the chiral asymmetry takes the value α at time t . Using this equation, they derived an expression for the selection probability to have a certain homochiral state which depends on the initial distribution of α .

From a different perspective, Gaspard has been working on a stochastic description of co-polymerisation processes [41, 42]. These pioneering studies paved the road toward a new approach to co-polymerisation. Indeed, previous studies were considering fully irreversible growth regimes where a monomer is attached to the end of the growing co-polymer but its detachment was neglected [43, 44]. Moreover, these works were essentially following a macroscopic description of the co-polymerisation. His first paper on the subject was mainly motivated by the understanding of the influence of a detachment rate comparable to the attachment rate on the growth of a co-polymer [41]. The central assumption of his study was to consider that these rates only depend on the last monomeric unit present at the tip of the chain. Using this assumption and from the ensuing kinetics, he demonstrated that a co-polymer chain undergoing such a growth mechanism was exactly following the behaviour of a first-order Markov chain, thus allowing him to derive some thermodynamic features like the entropy production or the affinity associated to the growth process. Since it has been shown that the growth of DNA can be associated to the same kind of attachment-detachment process [45]. Afterwards, he extended his study to another particular case where the rates do not depend on the last monomeric unit. A co-polymer undergoing such a growth mechanism is called a Bernoulli chain. Later, he pushed forward his study by generalising the growth to a k^{th} -order Markov chain where the k last monomeric units influence the attachment-detachment rates [42].

3. Stochastic behaviour of copolymerisation processes

As described in the previous section of this overview, numerous theoretical models have

been proposed to investigate the emergence of homochirality in various chemical systems among different research fields such as crystallization processes, organic chemistry, and polymerisation reactions.

However, the connection between the microscopic growth mechanisms of chiral macromolecules (such as DNA) and the corresponding macroscopic properties has not yet been elucidated. Motivated by this unresolved question, the author's master thesis aimed to clarify this link by proposing a new approach to chiral copolymerisation processes. To do this, a new model has been proposed involving different growth mechanisms of a chiral chain from achiral monomers.

3.1. A new model for co-polymerisation processes

The model can be briefly summarized as follows: (i) An achiral monomer A is adsorbed on an activated site and adopts a certain conformation R or S as a result of the adsorption process, (ii) this species becomes an initiator site with which a new achiral monomer A will be able to react. Similar to the initial adsorption, the newly attached monomers become chiral as a consequence of the addition reactions. The combination of these two processes leads to the gradual growth of the polymer chain with different enantiomeric compositions. All the processes involved are considered fully reversible.

Inspired by Gaspard's works, two distinct growth mechanisms have been investigated: 1) A first mechanism in which the addition of a monomer is totally arbitrary, referred to as "Bernoulli's growth" and 2), a second mechanism where the activated chiral monomer at the growing tip of the polymer chain favors the addition of a monomer with the same chirality, referred to as "Markov's growth".

During the master thesis, the corresponding macroscopic behaviors have been studied through the construction and numerical integration of evolution equations describing the evolution in

time of the enantiomeric composition. Then, a more microscopic description has been used to evaluate the distribution of probability associated to each growth mechanism. Finally, stochastic simulations have been performed using Gillespie's algorithm to compare the results with the prediction from the previous analysis.

3.2. Importance of the description scale

First, it has been shown that the macroscopic description, which remains the most common approach for these kinds of problems, can provide misleading information about the chirality of the resulting polymers. Our microscopic description has made it possible to demonstrate that certain mechanisms lead to a population of racemic chains (50% of R monomers and 50% of S monomers in each chain), while others give rise to two equivalent populations of homochiral polymers. (100% of R or 100% of S in each chain). The macroscopic approach, which only concerns the average of the population, does not make it

possible to distinguish these two cases which are intrinsically different in terms of chirality. It is therefore not, in this sense, a relevant tool for detecting the emergence of homochirality.

3.3. Fluctuation-driven growth

The microscopic approach revealed that polymers can grow even when the macroscopic approach predicts that they cannot. This growth is due to the presence of fluctuations in the rates of the processes, which are a signature of the deeply probabilistic character of the dynamics of the system. It is observed for all the mechanisms considered and is probably universal. Such growth would be possible thanks to the free energy associated with the gain of configurations accessible by a growing chain. Indeed, the entropy associated to the variability of the chains' composition might contribute to the driving force (the *affinity*) of the growth process. This has already been suggested during the analysis of general fluctuating co-

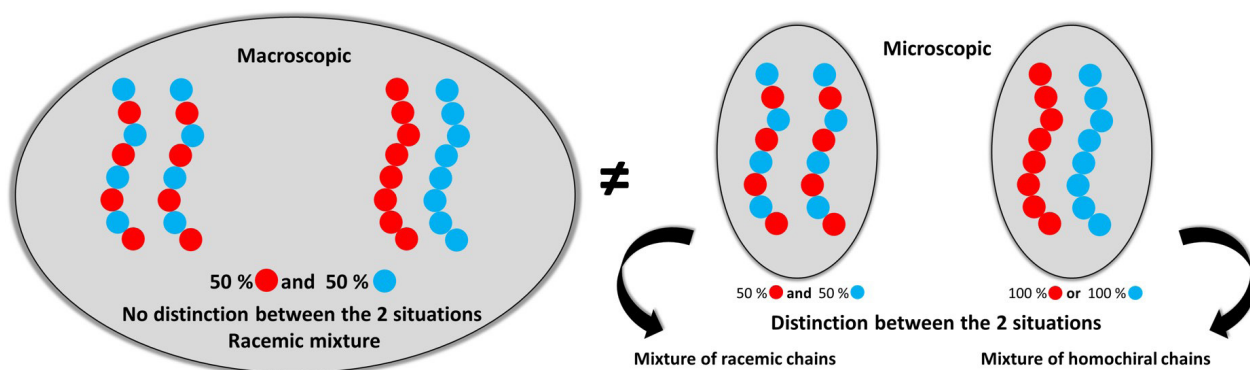


Figure 9. Schematic representation of the importance of description scale.

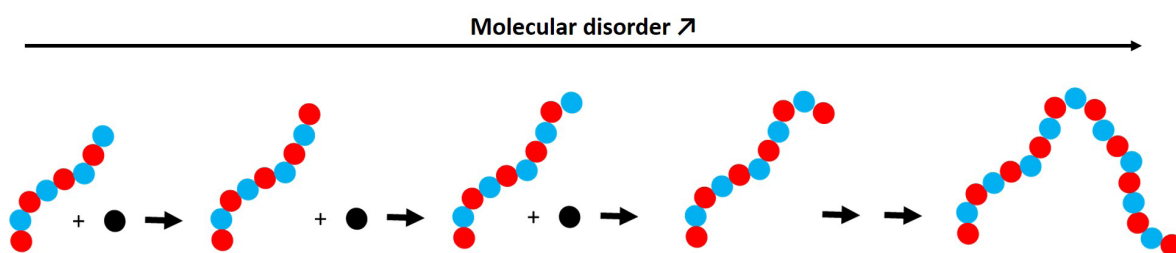


Figure 10. The gradual addition of monomers increases the number of possible configurations of the chain and thus, its entropy.

polymerisation processes [46]. In their study, Andrieux and Gaspard showed that the rate of entropy production during for the growth of a co-polymer obeys the relation:

$$\frac{1}{k_b} \frac{d_i S}{dt} = v \mathcal{A} = v (\varepsilon + D) \geq 0$$

where v is the mean velocity, ε is the free-energy parameter per monomer and D , the Shannon parameter, which measures the disorder in the chain due to its growth. Thus, it would seem that the quest for “disorder” is an engine for the growth of such polymer chains.

3.4. Formation of homochiral oligomers

A new path towards the formation of small homochiral polymers has been demonstrated by our stochastic approach. Certain growth mechanisms give rise to polymers which are racemic, but composed of long homochiral segments. The recombination of such segments could give rise to long homochiral polymers, such as those observed in the living world. These results may open new horizons for understanding the emergence of homochiral molecules essential to life, such as DNA or proteins.

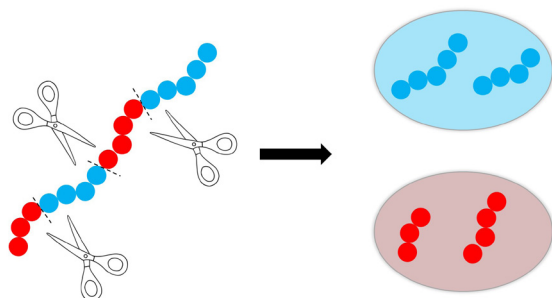


Figure 11. Homochiral segments can be isolated as homochiral oligomers.

4. Hydrodynamics & homochirality – a new pathway to chiral amplification?

Inspired by the experiments mentioned in this overview, numerous theoretical models have been developed to understand the underlying mechanisms but none of these explicitly considers the effect of transport phenomena such as diffusion or natural convection. However, as highlighted by Viedma's work, it is fair to

suspect that these processes are involved in the amplification mechanism.

Thanks to a F.R.S-FNRS funding, the author has the opportunity to explore this last hypothesis during his thesis under the supervision of Pr. Laurence Rongy and Pr. Yannick De Decker, from the Université libre de Bruxelles.

The main aim of this recently started thesis is to investigate the effect of transport phenomena on the amplification of an enantiomeric excess toward homochirality. More precisely, the influence of diffusion, advection and hydrodynamic instabilities on the selection and the amplification of a chiral state will be investigated. Kinetic reaction-diffusion-convection simulations will be performed in order to (i) assess the importance of different transport phenomena on the amplification of an enantiomeric excess, and (ii) reproduce key experimental results of the literature and provide new experimental perspectives for the deracemization of chiral compounds. The effect of temperature and heat of reaction, as well as the role of transport phenomena on the attrition-decomposition of chiral clusters, will also be investigated.

In such a way, chemical processes of high interest such as the emergence of homochirality near submarine hot springs in the early instants of life on earth, enantioselection during organic synthesis or homochiral self-assembled materials could be studied with a realistic theoretical approach that includes transport phenomena. From another perspective, microscopic extensions could be considered regarding the possible stochastic behaviours behind the symmetry breaking process.

5. Conclusion

As illustrated in this overview, chirality and homochirality have not revealed all their secrets yet. The emergence of single-handedness in nature is still an enigma which continues to puzzle many scientists. This research field shows once more that interdisciplinary scientific collaboration is the key to move forward.

Theoretical works along experimental evidences feed each other to provide insights regarding the unsolved questions surrounding us.

The interested reader can find additional information in some of the most recent reviews on the subject [6, 13, 47].

6. Acknowledgements

The author would like to thank the SRC to give him the opportunity to share his work performed

in the framework of his master thesis. The author thanks the FRS-F.N.R.S for the funding of his recently started PhD thesis. Finally, the author would like to thank the supervisors of his various works, L. Rongy and Y. De Decker.

This publication is supported by the French Community of Belgium within the framework of the financing of a FRIA grant.

Cette publication bénéficie du soutien de la Communauté française de Belgique dans le cadre du financement d'une bourse FRIA.

References

- [1] L. Pasteur, C. R. T. 26 (1848) 535.
- [2] Société chimique de Paris., (1863) 87 v.
- [3] J.P. Lotsy, J. Bosscha, E.H. von Baumhauer, Hollandsche Maatschappij der Wetenschappen., (1866) 45 v.
- [4] W.T. Kelvin, *The Molecular Tactics of a Crystal*, Oxford, Clarendon Press, 1894.
- [5] R.S. Cahn, C. Ingold, V. Prelog, *Angewandte Chemie International Edition in English* 5 (1966) 385–415.
- [6] T. Buhse, J.-M. Cruz, M.E. Noble-Terán, D. Hochberg, J.M. Ribó, J. Crusats, J.-C. Micheau, *Chem. Rev.* (2021).
- [7] F.C. Frank, *Biochimica et Biophysica Acta* 11 (1953) 459–463.
- [8] M. Calvin, *Chemical Evolution*, UK: Oxford University Press, 1969.
- [9] D.K. Kondepudi, G.W. Nelson, *Phys. Rev. Lett.* 50 (1983) 1023–1026.
- [10] P. Decker, *J Mol Evol* 2 (1973) 137–143.
- [11] K. Iwamoto, *Phys. Chem. Chem. Phys.* 5 (2003) 3616–3621.
- [12] K. Asakura, A. Ikumo, K. Kurihara, S. Osanai, D.K. Kondepudi, *J. Phys. Chem. A* 104 (2000) 2689–2694.
- [13] R. Plasson, D.K. Kondepudi, H. Bersini, A. Commeyras, K. Asakura, *Chirality* 19 (2007) 589–600.
- [14] null Green, null Park, null Sato, null Teramoto, null Lifson, null Selinger, null Selinger, *Angew. Chem. Int. Ed. Engl.* 38 (1999) 3138–3154.
- [15] P.G.H. Sandars, *Orig Life Evol Biosph* 33 (2003) 575–587.
- [16] Y. Saito, H. Hyuga, *J. Phys. Soc. Jpn.* 74 (2005) 1629–1635.
- [17] D.K. Kondepudi, R.J. Kaufman, N. Singh, *Science* 250 (1990) 975–976.
- [18] K. Soai, S. Niwa, H. Hori, *J. Chem. Soc., Chem. Commun.* (1990) 982–983.
- [19] D.K. Kondepudi, K. Asakura, *Acc. Chem. Res.* 34 (2001) 946–954.
- [20] K. SOAI, *Proc Jpn Acad Ser B Phys Biol Sci* 95 (2019) 89–110.
- [21] C. Viedma, *Phys. Rev. Lett.* 94 (2005) 065504.
- [22] W.L. Noorduin, E. Vlieg, R.M. Kellogg, B. Kaptein, *Angewandte Chemie International Edition* 48 (2009) 9600–9606.
- [23] L.-C. Sögütoglu, R.R.E. Steendam, H. Meekes, E. Vlieg, F.P.J.T. Rutjes, *Chem. Soc. Rev.* 44 (2015) 6723–6732.
- [24] W.L. Noorduin, B. Kaptein, H. Meekes, W.J.P. van Enkevort, R.M. Kellogg, E. Vlieg, *Angewandte Chemie International Edition* 48 (2009) 4581–4583.
- [25] I. Baglai, M. Leeman, R. M. Kellogg, W. L. Noorduin, *Organic & Biomolecular Chemistry* 17 (2019) 35–38.
- [26] A. Lennartson, M. Håkansson, *Angewandte Chemie International Edition* 48 (2009) 5869–5871.
- [27] A. Lennartson, S. Olsson, J. Sundberg, M. Håkansson, *Angewandte Chemie International Edition* 48 (2009) 3137–3140.
- [28] S.B. Tsogoeva, S. Wei, M. Freund, M. Mauksch, *Angewandte Chemie International Edition* 48 (2009) 590–594.
- [29] A.M. Flock, C.M.M. Reucher, C. Bolm, *Chemistry – A European Journal* 16 (2010) 3918–3921.
- [30] M. Sakamoto, F. Yagishita, M. Ando, Y. Sasahara, N. Kamataki, M. Ohta, T. Mino, Y. Kasashima, T. Fujita, *Org. Biomol. Chem.* 8 (2010) 5418–5422.
- [31] F. Yagishita, H. Ishikawa, T. Onuki, S. Hachiya, T. Mino, M. Sakamoto, *Angewandte Chemie International Edition* 51 (2012) 13023–13025.
- [32] R.R.E. Steendam, M.C.T. Brouwer, E.M.E. Huijs, M.W. Kulka, H. Meekes, W.J.P. van Enkevort, J. Raap, F.P.J.T. Rutjes, E. Vlieg, *Chemistry – A European Journal* 20 (2014) 13527–13530.
- [33] D.T. McLaughlin, T.P.T. Nguyen, L. Mengnjo, C. Bian, Y.H. Leung, E. Goodfellow, P. Ramrup, S. Woo, L.A. Cuccia, *Crystal Growth & Design* 14 (2014) 1067–1076.
- [34] M. Uwaha, H. Katsuno, *Journal of the Physical Society of Japan* 78 (2009) 023601.
- [35] J.M. McBride, J.C. Tully, *Nature* 452 (2008) 161–162.
- [36] Z. El-Hachemi, J. Crusats, J.M. Ribó, S. Veintemillas-Verdaguer, *Crystal Growth & Design* 9 (2009) 4802–4806.
- [37] C. Viedma, P. Cintas, *Chem. Commun.* 47 (2011) 12786–12788.
- [38] K. Suwannasang, A.E. Flood, C. Rougeot, G. Coquerel, *Crystal Growth & Design* 13 (2013) 3498–3504.
- [39] K. Suwannasang, G. Coquerel, C. Rougeot, A.E. Flood, *Chemical Engineering & Technology* 37 (2014) 1329–1339.
- [40] D.K. Kondepudi, G.W. Nelson, *Nature* 314 (1985) 438–441.
- [41] P. Gaspard, D. Andrieux, *J. Chem. Phys.* 141 (2014) 044908.
- [42] P. Gaspard, *Journal of Statistical Physics* 164 (2016) 17–48.
- [43] F.R. Mayo, F.M. Lewis, *J. Am. Chem. Soc.* 66 (1944) 1594–1601.
- [44] T. Alfrey, G. Goldfinger, *J. Chem. Phys.* 12 (1944) 205–209.
- [45] K.A. Johnson, *Annu. Rev. Biochem.* 62 (1993) 685–713.
- [46] D. Andrieux, P. Gaspard, *Proceedings of the National Academy of Sciences of the United States of America* 105 (2008) 9516–21.
- [47] Y. Saito, H. Hyuga, *Rev. Mod. Phys.* 85 (2013) 603–621.

Tom CARDEYNAELS

Hasselt University, Institute for Materials Research (IMO-IMOMEC),
Design & Synthesis of Organic Semiconductors (DSOS), Agoralaan
1, 3590 Diepenbeek, Belgium
University of Namur, Laboratory of Theoretical Chemistry,
Theoretical and Structural Physical Chemistry Unit, Namur Institute
of Structured Matter, Rue de Bruxelles 61, 5000 Namur, Belgium
tom.cardeynaels@uhasselt.be

An overview of organic light-emitting diodes: from past generations to modern light emission principles

This article is part of the PhD Thesis of the author, realized under the joint supervision of W. Maes (UHasselt) and B. Champagne (UNamur), and defended on November 27th 2020.

Abstract

Organic light-emitting diodes (OLEDs) have entered our everyday life as we can nowadays find them in smartphone and television screens. Their widespread use can be attributed to their ability to outperform technologies based on classical semiconductors, whereas this is not possible or not yet achieved in other fields of organic optoelectronics such as solar cells. Current OLED efficiencies, i.e. the light output versus the power input, match or even surpass those of inorganic LEDs. Furthermore, the ability for ultra-thin processing and direct color emission, instead of having to rely on liquid crystals, makes them very successful in display technologies. Herein, a brief historic overview of the development of OLEDs is given with a focus on the organic emitters designed for the different OLED 'generations'. At the end, a short summary of our contributions to the field – joint computational/synthetic efforts on donor-acceptor chromophores displaying thermally activated delayed fluorescence (TADF) – is provided as well.

1. 1st Generation OLEDs

Organic light-emitting diodes (OLEDs) have come a long way since the discovery of electroluminescence in 1936 [1], when Destriau showed that ZnS can emit light when an electric field is applied. In 1953, Bernanose *et al.* for the first time observed electroluminescence in organic materials by introducing acridine orange (Figure 1) in a cellulose matrix and applying an alternating electric field.[2]. 10 years later, Pope *et al.* placed a layer of single crystal anthracene between two silver electrodes and applied a voltage to it (Figure 1) [3]. At over 400 V, the result was a faint, but typical emission for anthracene. When anthracene was mixed with tetracene, the fluorescence emission of tetracene was observed.

In 1987, Tang and VanSlyke created the first electroluminescent device that paved the way for modern-day OLEDs at the Eastman Kodak Company (Figure 2) [4].

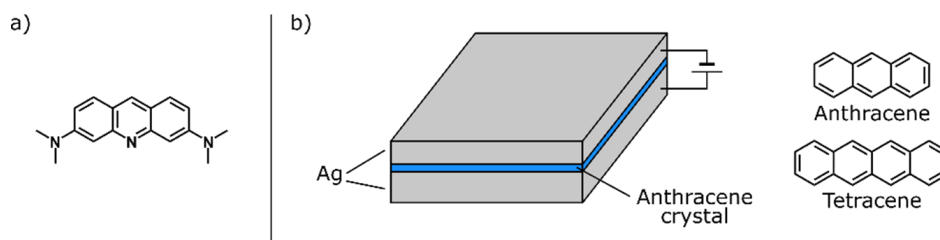


Figure 1. Molecular structure of acridine orange (left) and the device architecture and active materials used by Pope *et al.* [3] (right).

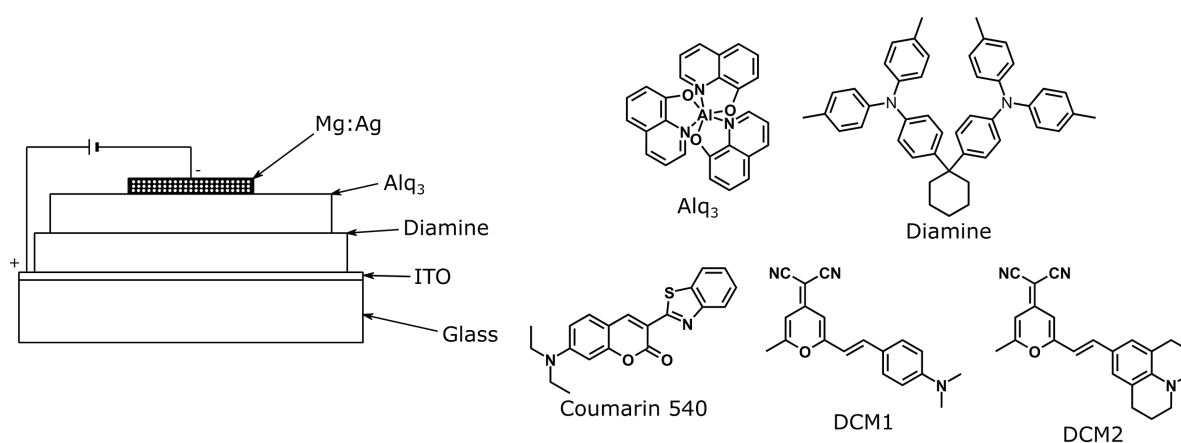


Figure 2. Device architecture applied by Tang and VanSlyke and molecular structures of Alq₃, the diamine layer and the colored emitters coumarin 540, DCM1 and DCM2 [4, 5].

Reproduced from ref. 4, with the permission of AIP Publishing.

They described their device as being a double layer diode, wherein two organic layers consisting of Alq₃ and a diamine were used. Alq₃ acts as a green emitter, whereas the diamine layer is used for monopolar charge carrier (hole) transport. Around the same time, Adachi *et al.* published a series of papers in which they expanded the device structure to three layers, including hole transport (HTL) and electron transport layers (ETL) between which the emitting layer is sandwiched [6, 7]. Various emitter materials such as anthracene, coronene and perylene [6] and a 12-phthaloperinone derivative [7] were used. The two-layer architecture from Tang and VanSlyke worked rather well because the emitters have relatively good electron-transporting properties. Switching to the three-layer architecture removed this need as both barrier layers provide enhanced charge carrier transport and so the pool of emitter materials could be expanded.

Adachi and coworkers further illustrated this by incorporating a hole transport layer with emitting properties, effectively combining the emitter and hole-transporting layer into one [8].

In 1989, Tang *et al.* were able to reach substantial device efficiencies by sandwiching an Alq₃ layer doped with green and orange-red emitters between two layers of pure Alq₃ (Figure 2) [5]. The higher photoluminescence quantum yield (PLQY), *i.e.* the ratio of emitted to absorbed photons, of the doped films, 3 to 5 times larger with respect to that of pure Alq₃ (PLQY = 8%), was expected to afford an increased device performance. Whereas devices using Alq₃ as the sole emitter afforded an efficiency of 1%, the new sensitized devices reached up to 3%. The device efficiency is defined here as the ratio of the number of photons emitted by the device to the number of charges injected into the device.

In these types of sensitized devices, electrons and holes that are injected from the anode and cathode move through the device until they encounter each other and recombine to form excitons (*i.e.* bound electron-hole pairs). Device tuning, making use of additional layers such as the hole and electron transporting layers, ensures that the electrons and holes recombine in the so-called active layer. This active layer usually consists of a 'host' material, *i.e.* a large energy gap semiconducting material capable of transporting the charge carriers to their destination, and an emitting material, on which the charges recombine.

Soon afterwards, in 1990, Burroughes *et al.* took a different route with the advent of organic conjugated polymers [9]. Their work involved the synthesis of a poly(*p*-phenylene vinylene) (PPV) derivative (Figure 3). The main advantage foreseen for a polymer emitter would be an improvement of the device stability as small molecule devices often suffer from recrystallization and other structural changes. However, due to the insolubility of the final polymer, a precursor polymer had to be processed from solution onto the bottom electrode, which

itself was deposited on a suitable substrate, followed by a thermal annealing step in vacuum in which the final PPV structure is formed. Indium tin oxide (ITO) was chosen as the bottom contact because of its semi-transparency, whereas a thin layer of aluminum was used as the top contact. In this device architecture, the polymer acts as the host and emitter at the same time, allowing charge recombination to occur on the polymer chains, followed by exciton diffusion until they decay and light is emitted. Unfortunately, the device efficiencies only reached up to 0.05%, which was attributed to failures at the polymer/thin metal interface.

Since then, several strategies have been used to synthesize soluble, and thus readily processable, polymers for OLED applications. These strategies often encompass the incorporation of large, sometimes branched, aliphatic chains as these prevent stacking (and thereby emission quenching) between the conjugated polymer backbones. Other aromatic motifs such as thiophene, fluorene and phenylene have been used. Changing the polymer backbone leads to a variation in emission color, but could also lead to changes in device stability and

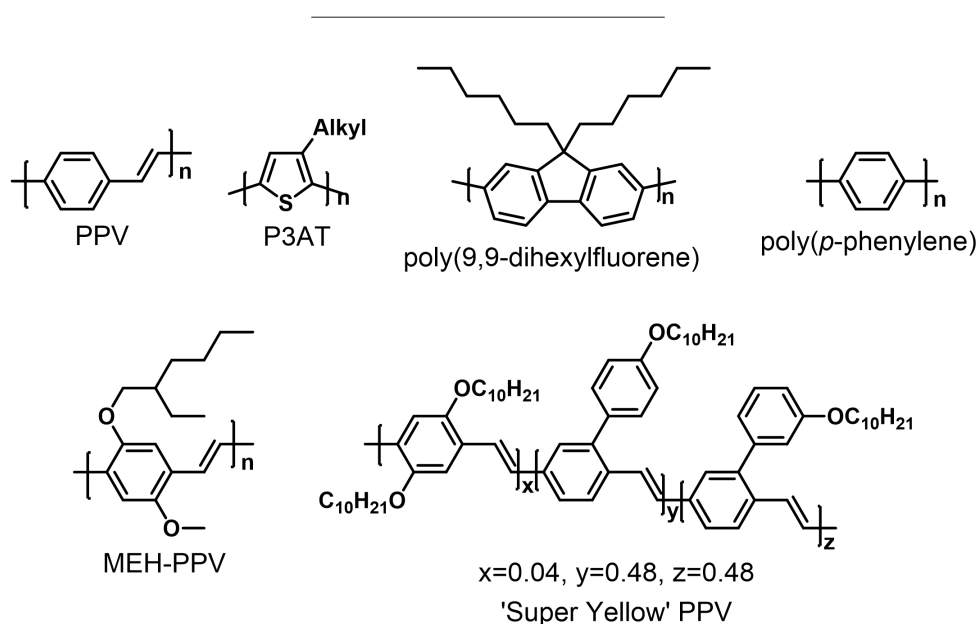


Figure 3. Polymer structures used in 1st generation OLED devices.

processability. Ohmori *et al.* (1991) made devices with poly(3-alkylthiophene) (P3AT) [10] and poly(9,9-dihexylfluorene) [11] as the active materials (Figure 3) because both polymers are well soluble with emission in the orange-red and blue, respectively. Unfortunately, efficiencies have not been reported for these devices. In 1992, Grem *et al.* prepared a poly(*p*-phenylene) (Figure 3) based device, similar to that of Burroughes *et al.*, in which a precursor polymer was processed and the final polymer was obtained after thermal annealing [12]. With blue emission, the device only managed to reach efficiencies of 0.01–0.05%, similar to the results with unfunctionalized PPV polymers. In the meantime, progress was made using PPV polymers and D. Braun and A.J. Heeger went on to functionalize the original PPV polymer with methoxy and 2'-ethylhexyloxy side chains to create poly(2-methoxy-5-(2'-ethylhexyloxy)-1,4-phenylene vinylene) or MEH-PPV (Figure 3) [13]. This functionalized PPV polymer has the benefit of being soluble in organic solvents, allowing facile processing without a thermal annealing step.

Development in the field of polymer OLEDs has continued, although polymers such as MEH-PPV are still being used as prototypical reference materials. One notable example is the PDY-132 developed by Merck Gmbh, which is also dubbed “super-yellow” (Figure 3) [14]. This PPV-based copolymer has a high PLQY in the yellow region and devices with 5.3% efficiency have been obtained, which is among the highest values reported for polymer-based OLEDs. Early incorporations of polymer OLEDs can be found in for example the Norelco electric shaver by Philips [15].

In addition to polymer OLEDs, researchers have investigated different ways of combining facile solution processing with excellent photophysical properties. Dendrimers can be designed to have extended π -conjugated structures, giving them semiconducting properties, but because of their branched nature, they are far more soluble than their polymer counterparts. Early designs were based on an emissive core surrounded by either a

fully conjugated or partially saturated periphery. Using conjugated or partially conjugated branches, the charge transport from the electrodes to the active material could be improved. In 1996, Wang *et al.* built a dendrimer around an anthracene unit using phenylene ethynylene units to create the branches (Figure 4) [16]. Unfortunately, the devices suffered from solid-state aggregation and self-quenching. Pillow *et al.* designed a dendrimer with a porphyrin core and stilbene branches (Figure 4), resulting in red emission [17]. Kwok and Wong used distyrylbenzenes with poly(benzyl ether) type dendritic wedges (Figure 4) [18]. Their dendrimer showed blue emission and despite its non-conjugated periphery, it was found that energy transfer does occur between the branches and the core. In 2003, six-arm star-shaped oligofluorenes were synthesized by Zou *et al.* (Figure 4), affording blue emission and a maximum device efficiency of 6.8% [19].

Despite substantial efforts towards solution-processable polymer and dendrimer OLEDs, small molecule OLEDs have remained the main area of interest. This is mainly due to the lower device efficiencies obtained using polymer and dendrimer active materials, which themselves are a result of device defects that are introduced via solution processing and defects in the polymer backbones introduced during their synthesis. Device defects occur as the hole/electron transporting/blocking layers are often small molecule organic materials, which can partially redissolve during the addition of novel layers, making pin-holes more likely and leading to a poor active layer morphology. In contrast to polymers, small molecule emitters can be readily purified using sublimation techniques and they allow device fabrication via vapor deposition, affording a higher degree of control over the layers and their morphology in multi-layer device stacks.

In the above section, a brief summary of the history of the first generation OLEDs, based on simple fluorescent emitters, is provided. While some historically important studies are mentioned, the overview on fluorescent OLEDs given here is far from exhaustive.

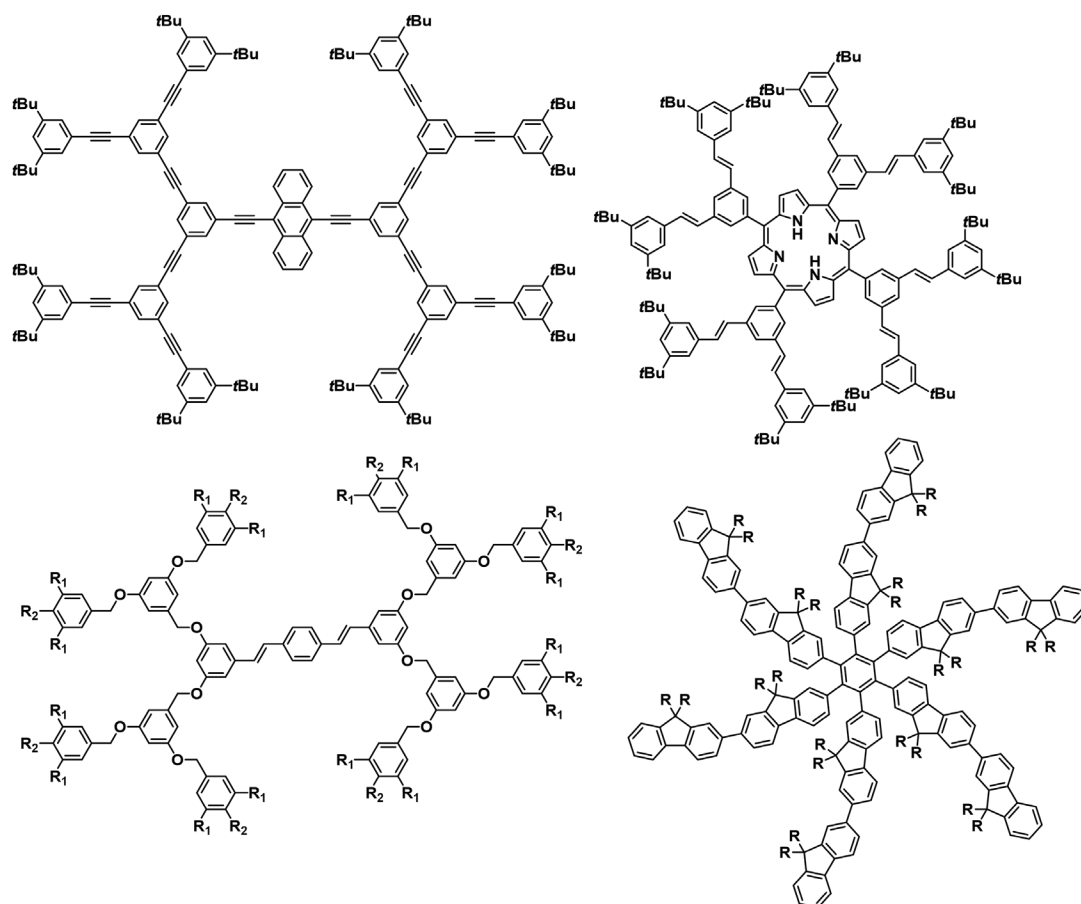


Figure 4. Dendritic active materials studied by Wang *et al.* [16] (top left), Pillow *et al.* [17] (top right), Kwok and Wong [18] (bottom left) and Zou *et al.* [19] (bottom right).

2. 2nd Generation OLEDs

Shortly after the initial discovery by Tang and VanSlyke [4], an alternative emission mechanism in the form of phosphorescence was used to develop OLED devices. Phosphorescence is the emission from the triplet state and is not commonly observed in organic fluorophores (*e.g.* in the materials from the previous section) (Figure 5). The underlying mechanism can be explained using quantum mechanics. For most organic materials, the ground state is of singlet nature. Absorption of a photon leads to excitation from the singlet ground state to one of the singlet excited states, depending on the energy of that photon. Because the excited triplet states have a different spin configuration, a change of spin is required to go from the singlet to the triplet state. Because of the laws of conservation of momentum, the change in spin angular momentum should be paired with a change of momentum elsewhere, typically in the

orbital angular momentum. Hence, the term spin-orbit coupling (SOC) is coined to describe the connection between the spin and orbital angular momentum in systems ranging from atoms to large organic compounds. Large SOC values are typically observed when heavy atoms such as lead (Pb), platinum (Pt) or iridium (Ir) are introduced, whereas intermediate values can be found for the heavy halogens iodine (I) and bromine (Br).

To reach the triplet state and subsequent emission back to the ground state, a certain amount of SOC is needed. The lack of SOC in common organic molecules, however, makes them unable to show phosphorescence. Furthermore, when an electron and a hole recombine in an OLED device, the formed exciton can be either of singlet or triplet nature. Because there is only one possible singlet and three possible triplet configurations, the excitons are formed in a ratio of 25% singlets and 75% triplets. Since phosphorescence is not

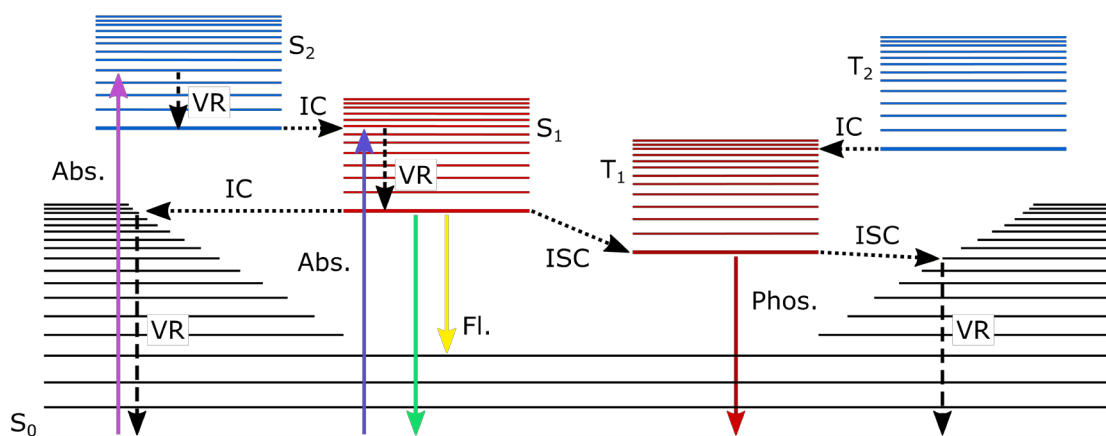


Figure 5. Jablonski diagram showing possible transitions. S_x and T_x = various singlet and triplet states; VR = vibrational relaxation; IC = internal conversion; ISC = intersystem crossing; Abs. = absorption; Fl. = fluorescence; Phos. = phosphorescence. The solid lines represent radiative transitions whereas the dashed lines represent non-radiative transitions.

possible for the 1st generation OLED emitters, the maximum internal quantum efficiency (IQE) can only be around 25% [20]. The EQE is dependent on the light outcoupling efficiency, in which nearly 75% of all emitted light is lost. Light outcoupling is mainly diminished by internal reflection and destructive interference within the OLED device [21].

The second generation OLED materials were designed to overcome these issues by the incorporation of heavy atoms. As they lead to an increase in spin-orbit coupling, giving rise to phosphorescence, intersystem crossing (ISC) becomes viable (Figure 5). The same SOC that leads to phosphorescence also enables ISC from the singlet to the triplet excited state. In an OLED device with such a heavy-metal containing emissive material, the 75% of triplet excitons that are inherently formed during charge recombination can now be exploited through the phosphorescent pathway. Subsequently, the 25% singlet excitons can be converted to the triplet state via ISC, leading to a maximal IQE of 100%. Nevertheless, even with an IQE of 100%, light outcoupling efficiencies of around 25% prevent EQEs of more than 25%.

In 1990, Kido *et al.* used a terbium (Tb^{3+}) complex of acetylacetonate to construct a two-layer device with $N^4, N^{4'}$ -diphenyl- $N^4, N^{4'}$ -di-*m*-

tolyl-[1,1'-biphenyl]-4,4'-diamine (TPD) as the hole-transporting layer (Figure 6) [22]. The device emitted green light with a very narrow spectral width, another advantage of using heavy-metal complexes making them ideally suitable for display applications. In 1993, Kido *et al.* reported on a red-emitting tris(thienyltrifluoroacetylacetonato) Eu^{3+} complex which was spin-coated in a poly(methylphenylsilane) film because it was not possible to evaporate this complex (Figure 6) [23].

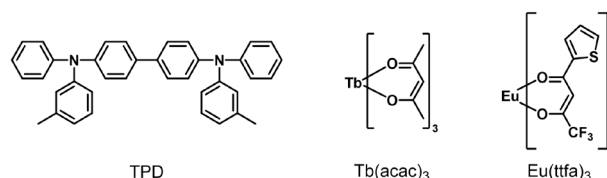


Figure 6. Terbium and europium complexes used by Kido *et al.*, with TPD as the hole-transporting material [22, 23].

These two complexes are among the first examples of heavy-metal complexes being applied to the field of OLEDs with the intent of boosting the device performance in terms of EQE and color purity. Baldo *et al.* used a phosphorescent 2,3,7,8,12,13,17,18-octaethyl-21*H*,23*H*-porphyrine platinum(II) (PtOEP) (Figure 7) dye as the emitter doped in Alq_3 [24]. With this combination, more than 90% energy transfer from the Alq_3 host to the porphyrin emitter was obtained, leading to an IQE and EQE of 23% and 4%, respectively. At the time,

this was a record efficiency for a red-emissive OLED. The same research groups then reported two more red-emitting porphyrin-based (Figure 7) OLEDs, again using Alq₃ as the host material [25]. 2,7,13,17-Tetraethyl-3,8,12,18-tetramethyl-21*H*,23*H*-porphyrine platinum(II) (PtOX) and 5,15-diphenyl-21*H*,23*H*-porphyrine platinum(II) (PtDPP) showed similar red-shifted emission as PtOEP, but with varying photoluminescence quantum yields. PtOX and PtOEP have quantum yields of 0.44 and 0.55, respectively, as expected due to the minimal structural change. PtDPP has a PLQY of only 0.16 as the phenyl groups on the porphyrin *meso*-positions likely lead to more non-radiative losses. As a result, the devices obtained with PtOX and PtOEP showed similar EQEs, whereas the devices containing PtDPP lagged behind.

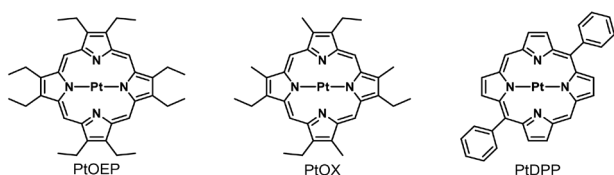


Figure 7. Phosphorescent Pt(II)-porphyrin emitters used by Baldo *et al.* [24] and Kwong *et al.* [25].

Introduction of a dopant into a host material was already described by Pope *et al.* as they showed doping of tetracene in anthracene gave predominant emission of the former [3]. Tang and VanSlyke used Alq₃ as a host for various fluorescent emitters [5] and the same host material was used for the porphyrin-based OLEDs by Baldo *et al.* [24] and Kwong *et al.* [25]. Doping of an emitter material in a suitable host has, in these examples, been shown to be advantageous for the overall efficiency of the devices. One of the key factors in achieving good efficiencies is a proper energy level alignment of the emitter and host molecules [26]. Ideally, the energy levels of the host encompass those of the emitter to ensure exciton formation on the dye molecules. In the case of exciton formation on the host molecules, exciton diffusion can occur and they will migrate to the dye, which essentially acts as an exciton trap (Figure 8). The emitter can therefore achieve higher IQE values as emission from the host or other device layers is minimized. Additionally, energy transfer from the host to the emitter should be as high as possible and ideally approach 100%.

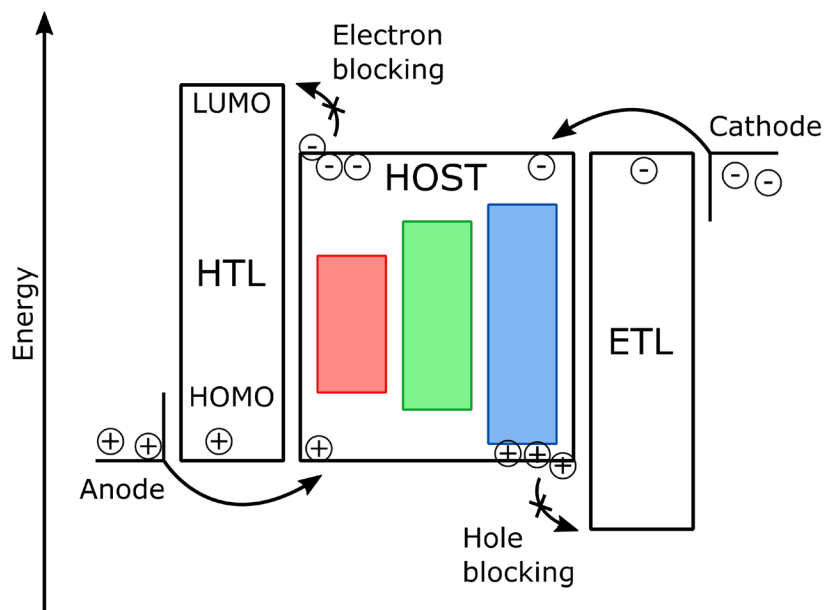


Figure 8. Simplified schematic of the energy levels in an OLED, ensuring exciton formation in the emitting layer. Adapted from *Journal of Chemical Information and Modeling*, 2018, 58, 2440-2449., with permission of the American Chemical Society [27].

Another advantage of using doping is that doped devices often give narrower electroluminescence than non-doped devices [26]. This is particularly interesting when looking at full color displays where mixing of the primary colors red, green and blue (RGB) is necessary to obtain white light. A lower color purity (*i.e.* broad emission) leads to washed out colors. Doping also enhances stability as the emitter is no longer crystalline and the ETL and HTL have less tendency to crystallize. As doping is typically done in low amounts (<20%), the emitter molecules experience less self-quenching and ultimately less material is needed to construct efficient devices. This is particularly useful as the emitter is usually the most expensive component of an OLED device.

The next important improvement on the device architecture came with the introduction of additional layers to enhance charge carrier confinement in the emitting layer and thereby improve the overall device efficiencies. Up until this point, only two-layer (hole-

transporting and emitting) or three-layer (hole and electron-transporting and emitting layer) architectures were used. Ikai *et al.* introduced a hole and exciton-blocking layer consisting of perfluorinated compounds in a four-layer architecture (Figure 9) [28]. The device consisted of electron (Alq_3) and hole ($\alpha\text{-NPD}$) transporting layers between which the hole/exciton-blocking layer and emitting layer are sandwiched. The hole/exciton-blocking layer is deposited between the emitting and electron-transporting layer to ensure that either holes or excitons are not able to migrate into the electron-transporting layer for charge recombination or relaxation (Figure 9).

This is possible due to the low-lying highest occupied molecular orbital (HOMO) and lowest unoccupied molecular orbital (LUMO) which are necessary for effective blocking of holes and injection of electrons, respectively. The green emitter tris[2-phenylpyridinato-C2,N] iridium(III), better known as $\text{Ir}(\text{ppy})_3$, was doped in 4,4',4''-tri(*N*-carbazolyl)triphenylamine (TCTA),

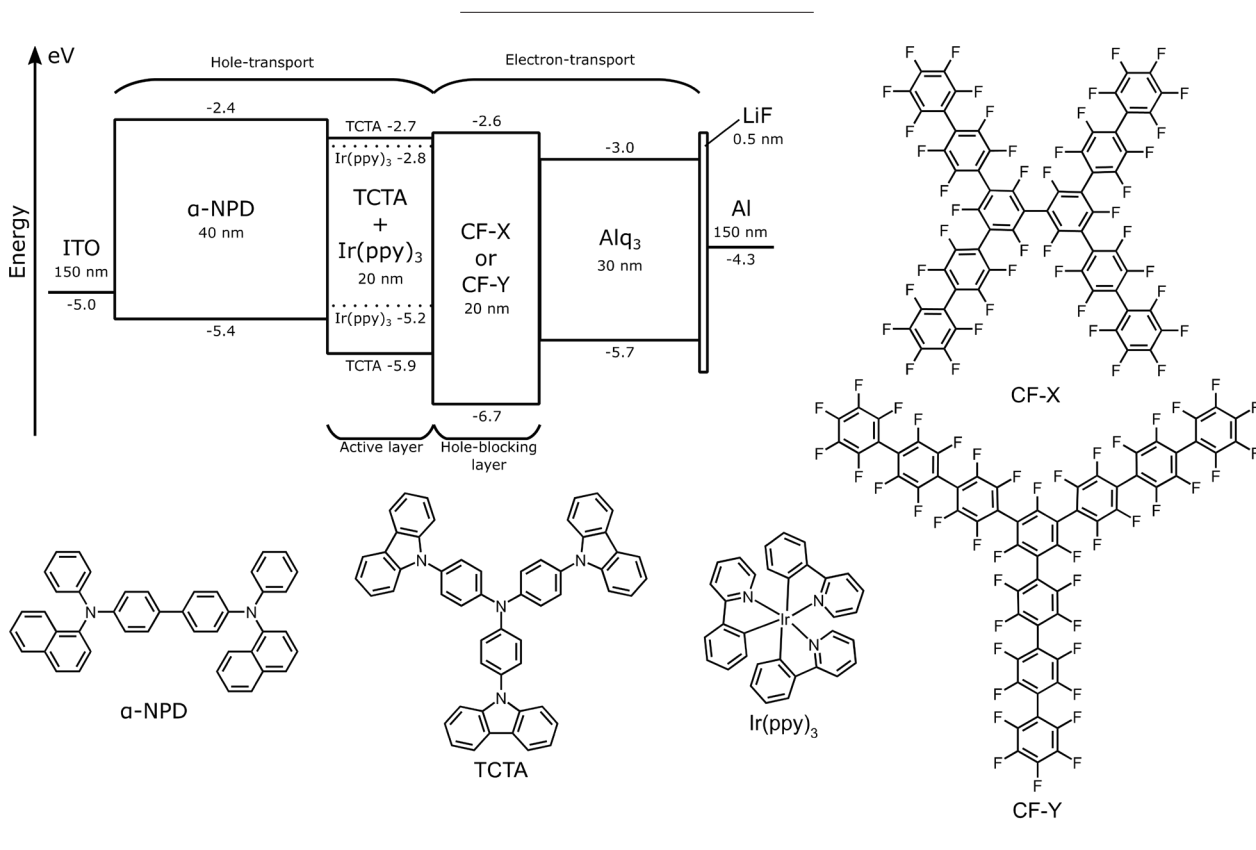


Figure 9. Device architecture and materials used in the work of Ikai *et al.* [28]. Adapted from *Applied Physics Letters*, 2001, 79, 156-158., with the permission of AIP Publishing.

which also has hole-transporting properties. Additional layers include an aluminum cathode, a lithium fluoride (LiF) electron injection layer and an ITO anode (Figure 9). EQEs of up to 19.2% were obtained using this device architecture.

Iridium arose as one of the most suitable heavy metals to obtain highly emissive complexes with color tuneability, owing to the strong SOC of the iridium atom and strong metal-ligand charge transfer. In 2001, Adachi *et al.* reported three novel iridium complexes with modified ligands to obtain blue-emissive complexes [29]. Due to the requirement of having high-energy singlet and triplet states, blue-emissive complexes are more difficult to obtain than their green or red counterparts. By gradually making the ligands more electron poor ($\text{Ir}(\text{ppy})_2(\text{acac})$ to $\text{Ir}(\text{Fppy})_2(\text{acac})$) and by switching an acetylacetonato ligand for a picolinate (FIrpic) (Figure 10), the emission was shifted from 516 to 465 nm in dilute chloroform solution. Using FIrpic, an EQE of $5.7 \pm 0.3\%$ was obtained, which was a significant improvement at that time for a blue emitter.

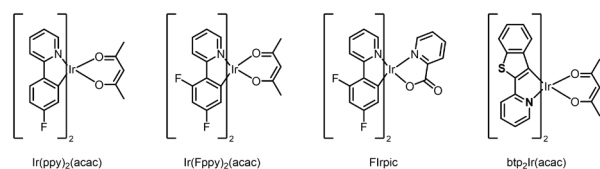


Figure 10. Iridium complexes reported by Adachi *et al.* [29, 30].

In the same year, Adachi *et al.* also reported on the highly efficient red-emitting complex bis(2-(2'-benzo[4,5- α]thienyl)pyridinato- N,C^3')iridium(acetylacetonate) [$\text{btp}_2\text{Ir}(\text{acac})$] (Figure 10) [30]. With an electroluminescence maximum at 616 nm, it comes close to the ideal color coordinates for video display standards. A maximum EQE of 7.5% was achieved, which is a significant increase over the 4% reported for the red-emitting PtOEP porphyrin (*vide supra*). Tuning of the emission color was further exploited by Tsuboyama *et al.*, who reported on a large number of red-emitting iridium complexes (Figure 11) in which the ligand character was made more donating or accepting depending on the addition of specific functional groups such as

methyl or CF_3 [31]. Varying the ligand strength not only changes the emission color, but also has implications on the phosphorescence quantum yield (ϕ_{ph}), as it changes the positions of the singlet and triplet energy levels. $\text{Ir}(\text{piq})_3$ was found to give very efficient red emission ($\lambda_{\text{max,Ph}} = 603 \text{ nm}$, $\phi_{\text{p}} = 0.26$) and a maximum EQE of 10.3 % [31].

Next to platinum and iridium-based complexes, other heavy metals such as ruthenium, osmium and rhenium have also been used [32]. Due to the higher oxidation potentials of these materials with respect to iridium, the prerequisites for the ligands are stricter and less design freedom is available. In combination with the (generally) higher EQEs for iridium-based devices, iridium has received most attention [33-36].

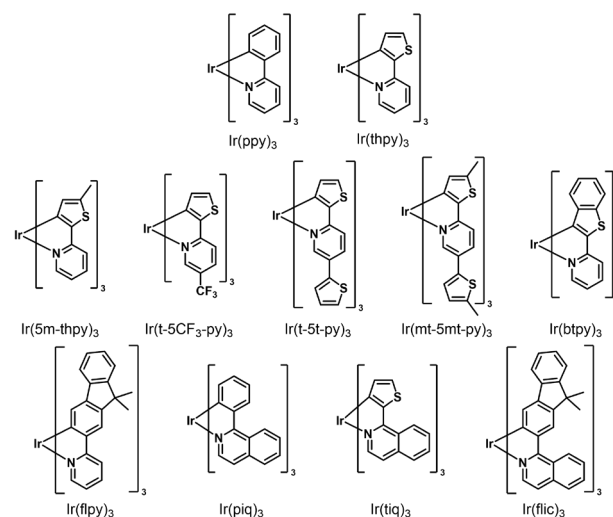


Figure 1. Iridium complexes synthesized by Tsuboyama *et al.* [31].

3. 3rd Generation OLEDs

The commercial success of the second generation OLEDs has inspired researchers to investigate the possibilities to further improve the device performance in terms of stability, lifetime and sustainability. Instead of utilizing the emissive triplet state, research has focused on upconversion of the triplet excitons to the singlet state. This can be achieved via triplet-triplet annihilation (TTA), thermally activated delayed fluorescence (TADF) or the hybrid locally excited charge transfer (HLCT) mechanism. The

most extensively studied mechanism is that of TADF and therefore, this is discussed in greater detail in this section.

3.1. The history of delayed fluorescence

The discovery of TADF dates back to the beginning of the 20th century. In 1929, Delorme and Perrin discovered delayed fluorescence emission from certain uranium salts, both in the solid state and in solution [37]. Measuring the emission of the salts at room temperature and at -180 °C (liquid oxygen), they observed a decrease in the emission lifetime, whereas the phosphorescence lifetime should go up upon decreasing the temperature. They therefore attributed the emission to some kind of delayed fluorescence. More than a decade later, Lewis *et al.* investigated the fluorescein molecule (Figure 12) in a solid state boric acid glass medium and found delayed emission by carefully looking at the emission and its lifetime at various temperatures [38]. In 1961, Parker *et al.* measured the time-resolved emission of eosin (Figure 12) in glycerol and ethanol and found the first example of temperature dependent delayed emission in solution [39].



Figure 12. Chemical structures of fluorescein, eosin Y and phenanthrene.

They found evidence for thermally activated ISC as well as direct ISC from an upper vibrational energy level of the singlet state to the triplet state. A prerequisite for these processes to occur efficiently is the proximity of the lowest excited singlet and triplet states, so that a small thermal barrier is left for either the ISC or the reverse ISC (rISC) process. The term E-type (E for eosin) delayed fluorescence was coined to describe the phenomenon. A year later, when investigating solutions of anthracene and phenanthrene (Figure 12), they observed similar delayed emission, but from singlet and triplet states that were further apart in energy. Therefore, a thermally activated process was ruled out. Instead, Parker *et al.* found

that triplet-triplet quenching (also known as TTA or triplet fusion) was most likely responsible for the formation of singlet excitons at very long lifetimes [40]. This phenomenon occurs when two excited molecules in the triplet state are in close proximity and energy transfer from one molecule to the other takes place. Two triplet excited states are converted to one singlet excited state and one molecule in the ground state, after which the singlet excited state can decay as delayed fluorescence. The process of TTA was originally named P-type delayed fluorescence after the molecule phenanthrene for which it was first discovered. TTA is here only mentioned because of its historical relevance. The detailed mechanism will be discussed later on when comparing the various triplet upconversion strategies.

Nishikawa *et al.* found E-type delayed fluorescence when trying to analyze porphyrinoid materials (Figure 13) based on their phosphorescence, but instead discovered delayed emission with a similar spectral position as the regular fluorescence [41, 42].

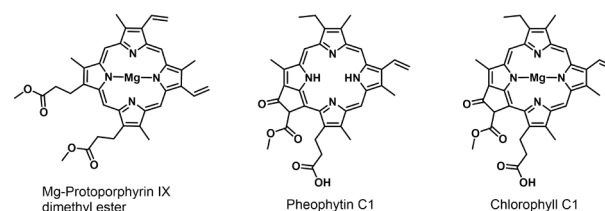


Figure 13. Porphyrinoids used by Nishikawa *et al.* [40, 41].

On top of the thermally activated nature, they postulated that the energy gap between the first excited singlet and triplet states should be less than 11 kcal mol⁻¹ (0.5 eV) as compounds exhibiting a larger singlet-triplet gap would not show delayed fluorescence [42]. Substituting the free-base porphyrins with a metal ion influences the rate of ISC and rISC according to the atomic number of the substituted metal ion, affording increased rates when going from H to Mg²⁺ and Zn²⁺. While E-type or thermally activated delayed fluorescence was found in numerous small molecules, such as the aforementioned ones but also in C70 fullerenes [43], benzophenones [44] and aromatic thiones [45], a suitable application was not found.

3.2. The theory of TADF

In 2009, Endo *et al.* discovered TADF in tin(IV)-porphyrins (Figure 14) and decided to implement them in OLED devices [46]. Their results were in line with the findings of Nishikawa *et al.* [42] that substituting the free-base porphyrins can lead to a significant increase in the observed TADF intensity. Although the compounds still contained a heavy-metal atom, this report sparked the interest in the field and the search for new TADF materials began as scientists started to understand the design principles behind TADF in fully organic molecules.

Following Endo's 2009 work on tin-porphyrins [46], the amount of literature on TADF increased significantly and fully organic emitters for OLED applications were reported soon thereafter. In 2011, the Adachi group published 2-biphenyl-4,6-bis(12-phenylindolo[2,3-*a*]carbazole-11-yl)-1,3,5-triazine (PIC-TRZ; Figure 15) as the first metal-free TADF compound for OLED applications, affording an EQE of 5.3% when doped in 1,3-bis(*N*-carbazolyl)benzene (mCP, 6 wt%) [47]. In the next two years, 10 reports with new emitters were published [48-57]. The best performing compounds from these reports are displayed in Figure 15 and some experimental

data are listed in Table 1. Although these data were obtained through varying methods for the different compounds, they provide a preliminary means of comparison. With EQEs ranging from 4.4% for the earliest work to >13% in the later studies, a huge improvement in OLED efficiency was already achieved. The emission maxima ranged between 485 and 553 for most of the materials and the compounds were largely green-yellow emitting. Only one blue OLED device (based on DBTDO-*t*BuCBZ) had been reported until this point, with red TADF OLEDs not being reported at all.

Compound	$\lambda_{\text{max,em}}^a$	ΔE_{ST} (meV) ^b	Max EQE (%)	Reference
PIC-TRZ	466	110	5.3	46
Spiro-CN	540	57	4.4	47
CC2TA	490	— ^c	11.0	48
SDB- <i>t</i> BuCbz	424	— ^c	9.9	49
PXZ-TRZ	544	— ^c	12.5	50
ACRFLCN	485	100	10.1	51
4CzIPN	508	83	19.3	52
2PXZ-OXD	517	150	14.9	53
DBTDO- <i>t</i> BuCbz	416	350	— ^c	56
tri-PXZ-TRZ	553	— ^c	13.3	54
ACRSA	494	30	16.5	55

Table 1. Overview of fully organic TADF reports from 2011-2013

- ^a Estimated from electroluminescence or doped-film photoluminescence spectra.
^b Calculated from the onset of the prompt fluorescence and phosphorescence or via an Arrhenius plot.
^c These values were not reported.

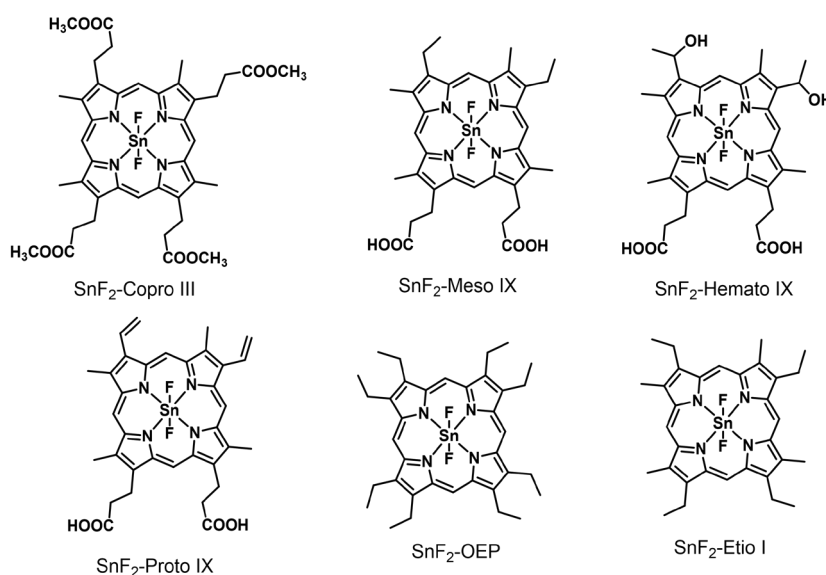


Figure 14. SnF₂-porphyrins used by Endo *et al.* to construct TADF-based OLEDs [45].

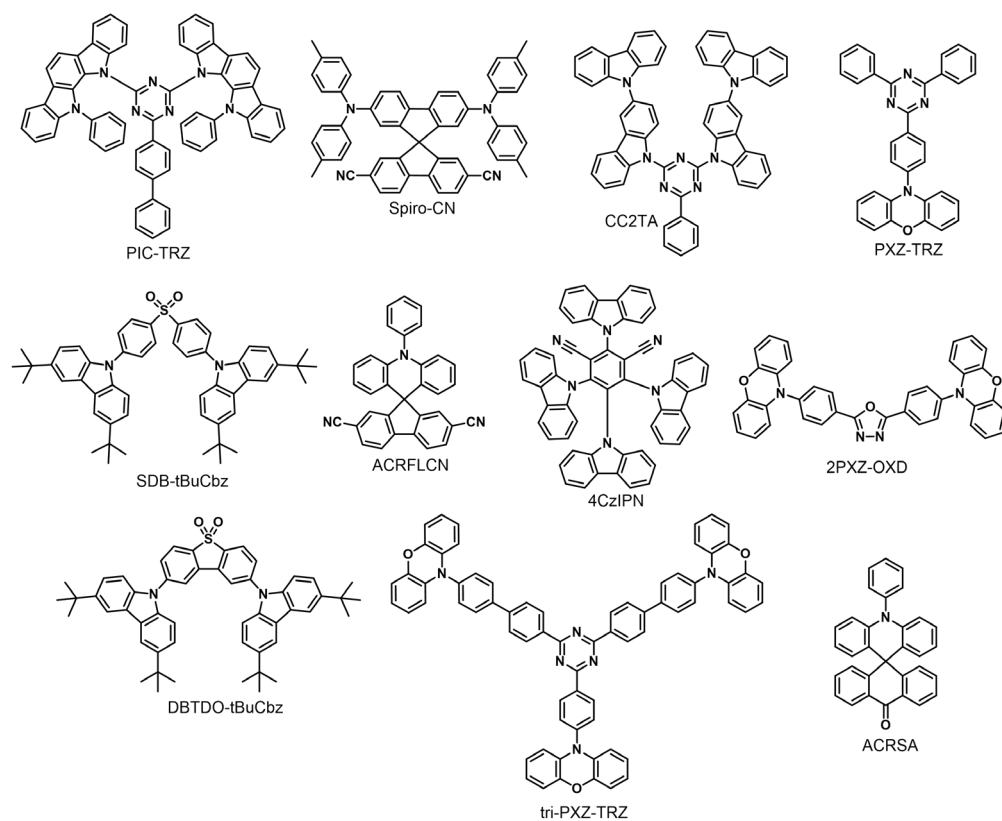


Figure 15. Chemical structures of the early full-organic TADF emitters listed in Table 1.

As was found by Parker *et al.* [39] and Nishikawa *et al.* [42], the mechanism of thermally activated delayed fluorescence relies on a series of excited state processes (Figure 16). When talking in terms of photoluminescence, a photon is absorbed and an electron is promoted from the (generally) singlet ground state to a singlet excited state according to the energy of the absorbed photon and the position of the singlet energy levels of the molecule in question. The excited state rapidly decays to the first excited singlet state in accordance to Kasha's rule [58], which states that internal conversion (IC) from a higher energy excited state to the lowest energy excited state of the same multiplicity occurs faster than any other excited state pathway. After the IC step, ISC from the singlet to the triplet state can occur. As previously discussed for the 2nd generation OLEDs, a change in the spin angular momentum has to be overcome by a change of orbital angular momentum through spin-orbit coupling. The use of heavy-metal atoms facilitates this transition due to

their inherently larger SOC effect. However, the compounds used by Parker *et al.* [39] and Nishikawa *et al.* [42] did not contain heavy-metal atoms. The intersystem crossing rate (k_{ISC}) is dependent on both the energy difference between the respective singlet and triplet states as well as the amplitude of SOC. A smaller energy difference between the singlet and triplet states leads to a larger k_{ISC} . Following the initial intersystem crossing, reverse ISC (rISC) can occur, whereupon the exciton goes from the triplet state back to the singlet state. Because the triplet configuration is generally lower in energy than the singlet configuration for a given state in organic compounds, this rISC process is endoenergetic and an energy barrier needs to be overcome. As the name TADF implies, this barrier is overcome using thermal energy. This also means the barrier cannot be too large. Whereas Nishikawa *et al.* postulated a barrier of approximately 0.5 eV [42], it should be at least below 0.2 eV for efficient rISC [59]. Once the exciton returns to its singlet configuration,

there are two options: either the exciton decays radiatively through fluorescence or it undergoes a second cycle of ISC/rISC. All these processes are dependent on their mutual rates. As was briefly touched upon, IC is typically very fast ($\ll 10^{-9}$ s), while fluorescence occurs at $\sim 10^{-9}$ s. ISC and rISC take place on much slower timescales of around 10^{-7} s and 10^{-6} – 10^{-5} s, respectively. The latter is especially slow due to the endoenergetic nature of the process. While phosphorescence is spin-forbidden, it is not entirely impossible. However, due to the SOC dependence, it occurs only at around 10^{-3} s. Given these rates, the rate of TADF is effectively governed by the rate of rISC, as it is the slowest step. Delayed emission in TADF emitters is therefore often observed in the microsecond domain [59]. As the singlet state from which radiative decay occurs is the

same for the prompt ($\sim 10^{-9}$ s) and the delayed ($\sim 10^{-6}$ s) emission, their spectral shape should be identical, as was observed by Parker *et al.* [39] and Nishikawa *et al.* [42], and led them to believe the observed delayed emission could not be coming from phosphorescence.

Moving to OLEDs, where excitons are formed by recombination of electrons and holes rather than via absorption of a photon, the processes involved are the same, with the exception that ISC is no longer a prerequisite for rISC to occur as the excitons are formed in a 25/75 ratio of singlets/triplets (Figure 16). Upconversion of the 75% formed triplet excitons via rISC gives TADF OLEDs the possibility to achieve up to 100% IQE. The former method of analysis via photon absorption rather than electrical

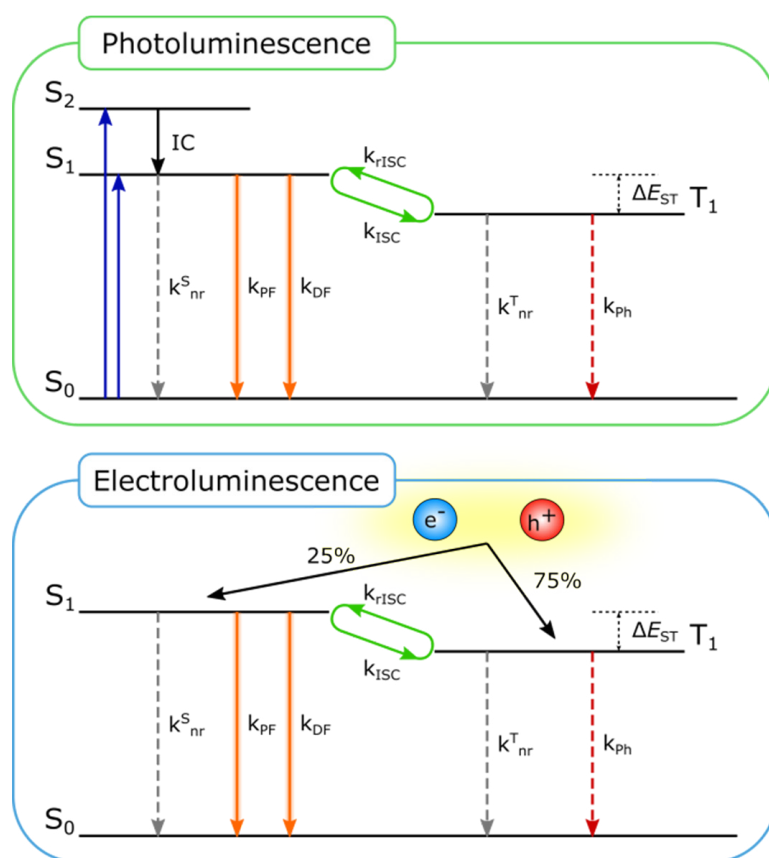


Figure 16. Schematic representation of the photophysical processes occurring upon photon absorption (top) or electrical excitation (bottom). IC = internal conversion, k_{nr}^S/k_{nr}^T = rate of non-radiative relaxation from the singlet or triplet state, k_{PF} = rate of prompt fluorescence, k_{DF} = rate of delayed fluorescence, k_{ISC}/k_{rISC} = rate of (reverse) intersystem crossing, k_{Ph} = rate of phosphorescence. Adapted from *Adv. Mater.*, 2014, 26, 7931–7958, with the permission of John Wiley and Sons.

excitation still plays a crucial role as potential emitters are typically characterized in this way before being tested in actual OLED devices. While we discussed the crucial excited state processes for efficient TADF, these are not the only possible pathways for the excitons to traverse along. Non-radiative transitions, such as IC, can also occur between the lowest excited singlet or triplet states and the ground state, resulting in a loss of the exciton energy without the irradiation of visible light. These non-radiative transitions are often coupled with vibrations, rotations of specific functional groups or the molecules as a whole and collisions with other molecules (*e.g.* in solution) need to be minimized. The key to avoiding these is making the molecule very rigid, so that the possibility for the vibrations and rotations to occur is very low. Therefore, in TADF design, as can be seen in Figure 15, the emitters generally consist of large conjugated and often heteroaromatic systems.

Next to being rigid, the key to designing efficient TADF emitters is to minimize the energy difference between the first excited singlet (S_1) and triplet (T_1) states. From quantum mechanics within the single transition approximation (STA), the singlet (ΔE_S) and triplet (ΔE_T) state energies can be written as Eq. 1.1 and 1.2, in which subscripts *i* and *a* are used to describe the occupied (often the highest, *i.e.* HOMO) and unoccupied (often the lowest, *i.e.* LUMO) molecular orbitals (MOs; φ), respectively. J_{ai} is the Coulomb interaction and K_{ai} is the exchange interaction between the occupied and unoccupied MOs. The energy difference ΔE_{ST} can then be written as Eq. 1.3. The value of K_{ia} is related to the overlap between φ_i and φ_a , as indicated in Eq. 1.4. Spatial separation of φ_i and φ_a should therefore lead to a small K_{ia} and hence a small ΔE_{ST}

$$\Delta E_S = {}^1\Delta E_{ai} = (\varepsilon_a - \varepsilon_i) - J_{ai} + 2K_{ai} \quad \text{Eq. 1}$$

$$\Delta E_T = {}^3\Delta E_{ai} = (\varepsilon_a - \varepsilon_i) - J_{ai} \quad \text{Eq. 2}$$

$$\Delta E_{ST} = {}^1\Delta E_{ai} - {}^3\Delta E_{ai} = 2K_{ai} \quad \text{Eq. 3}$$

$$K_{ai} = \iint dr dr' \varphi_a(r) \varphi_i(r) \frac{1}{|r-r'|} \varphi_a(r') \varphi_i(r') \quad \text{Eq. 4}$$

While the single-transition approximation presents limitations that are corrected using time-dependent density functional theory (TDDFT) calculations (most excited states have contributions from several single-particle transitions), it served as a first design criterion for novel TADF emitters.

In organic materials, the HOMO is typically located on the electron rich parts of the molecule, whereas the LUMO is typically located on the electron poor parts. By connecting an electron-rich moiety (often called electron-donating group or donor “D”) to an electron-deficient unit (often called electron-accepting group or acceptor “A”) via a covalent bond, localization of the frontier orbitals is only achieved to a given extent so that overlap remains present, leading to relatively large values of ΔE_{ST} . By spatially twisting the D and A groups in a molecule, the conjugation will decrease as the π -orbital overlap diminishes (Figure 17). This also leads to a better separation of the HOMO and LUMO [59]. Therefore, the most used strategy to obtain a small ΔE_{ST} is to provide sufficient steric hindrance between the D and A parts of a molecule to ensure a large dihedral angle between the two moieties [60]. Color tuning is then done by combining weaker or stronger donor or acceptor units to obtain more blue or red-shifted emission, respectively [61]. Alternatively, sp^3 -hybridized linkages such as a spiro conjugation can be applied as the lack of non-hybridized p-orbitals in an sp^3 -hybridized atom breaks up the conjugation and also leads to HOMO-LUMO separation (Figure 17) [62]. Unfortunately, a trade-off exists between the frontier orbital overlap and the rate of fluorescence (k_{pf}) [59]. The oscillator strength determines the strength of the coupling between the singlet ground and excited state. Excitations with a smaller oscillator strength show weaker absorption and emission intensity than excitations with a large oscillator strength. The size of the oscillator strength is determined by the overlap between the orbitals that are involved in the given transition. For a HOMO→LUMO transition for example, a large overlap between the HOMO and LUMO will lead to a large oscillator strength, if the symmetry conditions are also fulfilled, and a localized excited state (1LE state, superscript 1 for

singlet and 3 for triplet states), whereas a small overlap leads to a charge-transfer state (^1CT state, superscript 1 for singlet and 3 for triplet states) with a small oscillator strength. As the requirements for TADF include a small orbital overlap, typically for the HOMO and LUMO, these transitions are paired with a small oscillator strength, which is unfavorable for the fluorescence efficiency. Luckily, TADF emitters with a high k_{PF} and fluorescence quantum yield have been reported, indicating a less straightforward relationship between ΔE_{ST} and k_{PF} .

3.3. The spin-vibronic mechanism of TADF

Due to the structural design of TADF emitters, they often exhibit charge-transfer character in their transitions. Initially, the mechanism of TADF was therefore expected to result from direct (r)ISC between the first singlet and triplet excited CT states (*i.e.* ^1CT and ^3CT). However, the law of conservation of momentum forbids a change in spin angular momentum without a corresponding change in orbital angular momentum, or in other words, a $^1\text{CT} \rightarrow ^3\text{CT}$ transition between states of the same nature is not possible as there is no change in orbital angular momentum [63, 64], which is also known as El-Sayed's rule [63].

Hyperfine coupling induced ISC was proposed as an alternative mechanism based on time-resolved electron paramagnetic resonance (EPR) methods [65], but due to the small values for hyperfine interactions (HFI), usually in the range of 10^{-4} meV, it is unlikely that HFI alone can induce strong (r)ISC in these systems [66]. Furthermore, two experimental reports showed that the rate of reverse intersystem crossing (k_{rISC}) is not directly related to the size of ΔE_{ST} [67] and that, in some systems, it is possible to tune the excited states involved in the rISC step independently by changing the surrounding of the emitter [57, 68]. These findings lead to a more dynamic rISC process, which is not strictly governed by ΔE_{ST} and not strictly occurring between CT states. Chen *et al.* tried to calculate k_{rISC} occurring via SOC, but found a significant deviation from experimental values, even for the $^1\text{CT} \rightarrow ^3\text{LE}$ transition, which is allowed according to El-Sayed's rule [69]. Marian used multi-reference methods to show that direct SOC was too small to explain the efficient rISC observed in TADF, in agreement with the work by Chen *et al.* [69]. Instead, she proposed vibrational mixing between the ^3CT and an energetically close ^3LE state to be responsible for the efficient rISC [70-72]. Gibson *et al.* further elaborated on this and

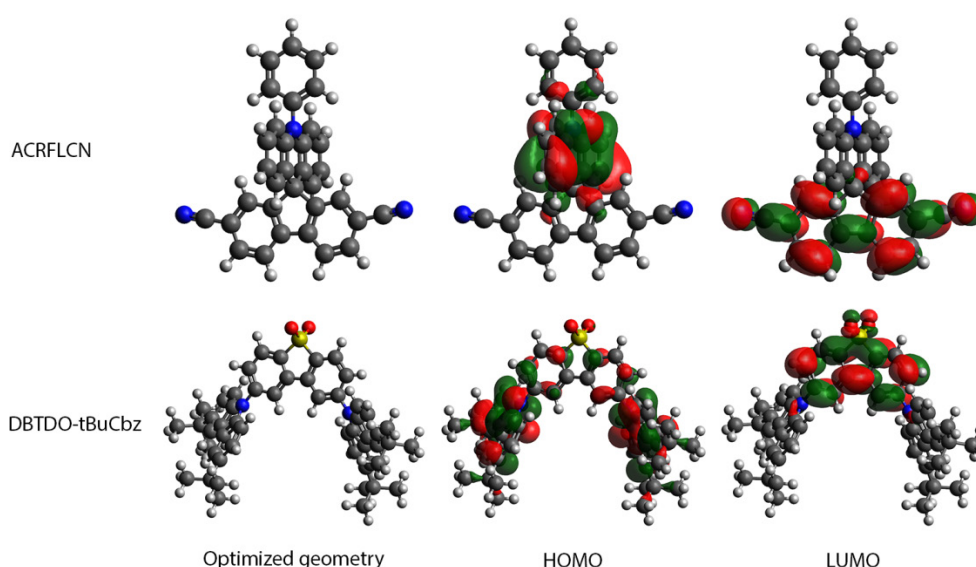


Figure 17. Optimized geometries, HOMO and LUMO topologies for a spiro conjugated (ACRFLCN) and a D-A based (DBTDO-tBuCbz) TADF emitter obtained using DFT (M06/6-311G(d)) (structures in Figure 15).

showed, through quantum dynamics simulations, the role of vibrational-electronic (vibronic) coupling of excited triplet states on k_{ISC} and k_{rISC} [66]. These results show how vibronic coupling helps to explain why compounds with an apparently large ΔE_{ST} can still show TADF.

Experimentally, ΔE_{ST} is obtained from the onset of the prompt fluorescence (singlet energy) at room temperature and delayed phosphorescence (triplet energy) at 80 K, both occurring from the lowest energy excited state for each multiplicity. The phosphorescence spectra are taken at 80 K because this transition is spin-forbidden and non-radiative losses dominate at room temperature. Decreasing the thermal energy and locking the conformation in a solid matrix allows the generally weak and red-shifted phosphorescence to be observed. The vibronic mechanism, however, couples the lowest excited triplet state to a higher energy excited triplet state to create ‘mixed’ states which are closer in energy to ^1CT . The energy gap that triplet excitons need to overcome to undergo rISC is therefore smaller than the experimental ΔE_{ST} (Figure 18) [60].

3.4. TADF emitters

In TADF literature, most reports deal with the design of novel (efficient) blue emitters. While 2nd generation phosphorescent OLEDs are commercially viable for green and red emission,

blue phosphorescent emitters suffer from instability due to the relatively weak metal-ligand bond and the inherently high triplet energy needed for blue emission. Blue TADF emitters might be able to overcome these issues, but their design is not straightforward. As mentioned before, blue CT emission can be achieved when relatively weak donor and acceptor units are coupled together. However, as their electron-donating and accepting properties become weaker, so does the CT character of their transitions and hence ΔE_{ST} becomes larger. Another issue is the use of 9,9-dimethyl-9,10-dihydroacridine (DMAC), 10*H*-phenoxazine (PXZ) or 10*H*-phenothiazine (PTZ) as the electron-donating groups. While these groups provide large steric hindrance and good HOMO/LUMO separation, their strong electron-donating properties red-shift the emission, often leading to a blueish/green emission. Similarly, when the acceptor unit is too strong, the emission is also red-shifted and becomes green or even yellow. This explains why the first reported TADF materials were predominantly green or yellow emitters (Table 1, Figure 15). Nonetheless, the design of blue emitters has been successful, as demonstrated by the large amount of entries in review articles, some of them affording OLEDs with EQEs above 20% [36, 61, 73-76]. Unfortunately, most blue TADF emitters still suffer from rapid and significant roll-off of the device efficiency and more research to find stable blue emitters is required [77-80].

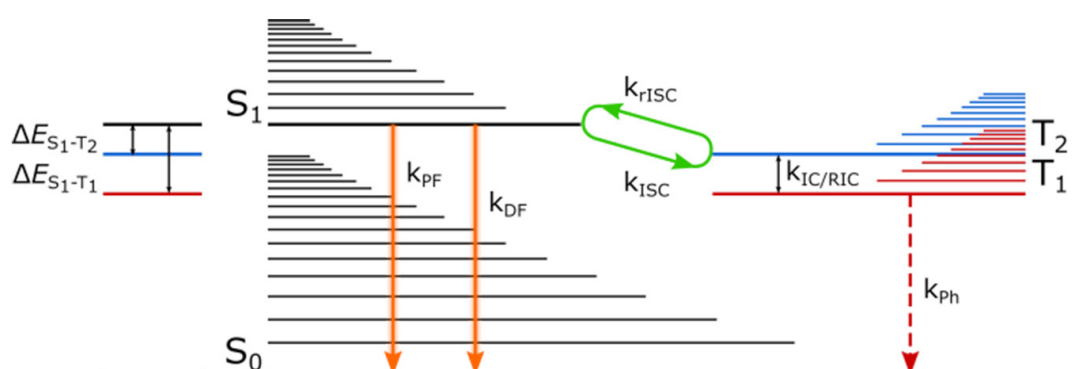


Figure 18. Schematic overview of the spin-vibronic mechanism for TADF. Vibronic coupling (VC) between T_1 and T_2 ensures population of the T_2 state regardless of the available thermal energy, resulting in a smaller effective ΔE_{ST}

Another consequence of having strong CT character is the inherent broadness of the CT emission ($\text{FWHM} > 50 \text{ nm}$), leading to reduced color purity, which is desired for OLED display applications. Recently, a new series of boron-based emitters has been proposed with extremely narrow ($\text{FWHM} < 30 \text{ nm}$) emission profiles [81-863]. These emitters have been termed multi-resonance (MR) TADF emitters as they allow for a small ΔE_{ST} , large k_{r} , high oscillator strengths and narrow emission via the opposing resonance effects of boron and nitrogen [81-83]. The emitters are based on the 5,9-diaza-13*b*-boranaphtho[3,2,1-*de*]anthracene (DABNA) core and afford deep-blue emission. Variations on this core have been made by incorporation of several peripheral groups (DABNA-1 and DABNA-2) [84], *tert*-butyl groups (*t*-DABNA) [85] or by fusing two DABNA cores together (*v*-DABNA) [86]. While these MR-TADF materials still suffer from rapid roll-off, they are among the best performing and most promising blue TADF-based OLED materials to date.

On the other end of the spectrum are the red TADF emitters. These have received less initial interest because there are sufficient red-emitting phosphorescent complexes available (Figure 11), affording OLEDs with decent EQEs. While red emitters do not suffer so much from instability issues, their PLQY is often much lower due to the so-called energy gap law [87, 88]. As the energy gap between the ground and excited state becomes smaller, non-radiative transitions become more plausible as the upper vibrational states of the electronic ground state start to overlap with those of the electronic excited states. Because of this,

the highest EQEs reported are in the range of 10-20%, with a few outliers above 20% [61, 89]. In 2018, Chen *et al.* reported a summary of red emitters with a maximum electroluminescence wavelength of 600 nm or larger [90]. Additionally, due to their fully organic, and thus non-toxic nature, they have found application in other fields outside of OLEDs. In 2014, Xiong *et al.* showed that a fluorescein derivative showing delayed fluorescence could be used for time-resolved fluorescence imaging in biological cells. Due to the long-lived nature, the cell autofluorescence dies out before the fluorescein delayed emission, enabling to enhance the imaging contrast [91]. Furthermore, the red-shifted emission of such materials makes them viable for operation in the so-called phototherapeutic window (600-1200 nm). Several other reports using TADF emitters for time-resolved imaging have been made since [92-97].

Similar to the first generation OLED materials, researchers have tried to incorporate the principles of TADF in other types of molecules such as dendrimers and polymers. The main advantages of dendrimer and polymer structures include facile processing via spin- or spray-coating for large area applications such as television screens and solid-state lighting [76]. Both fully and partially conjugated dendrimers have been made (Figure 20). In both cases, the dendrimer core consists of a TADF emitter which is responsible for the photophysical properties. The dendrons in conjugated dendrimers often consist of extended carbazole networks [98-101], whereas in partially conjugated dendrimers a short aliphatic chain connects the core with

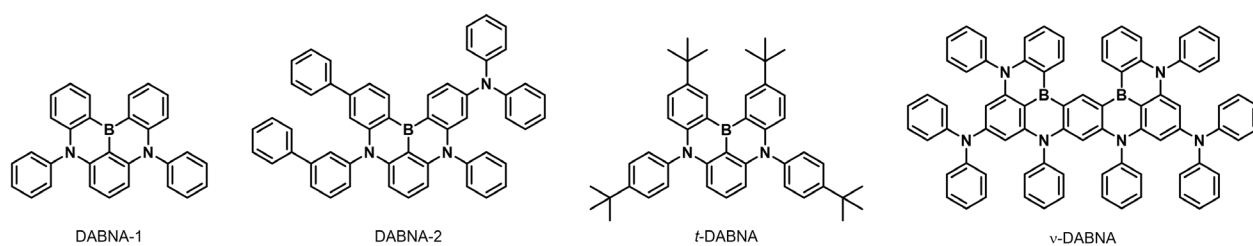


Figure 19. Chemical structures of some DABNA-based blue MR-TADF emitters [84-86].

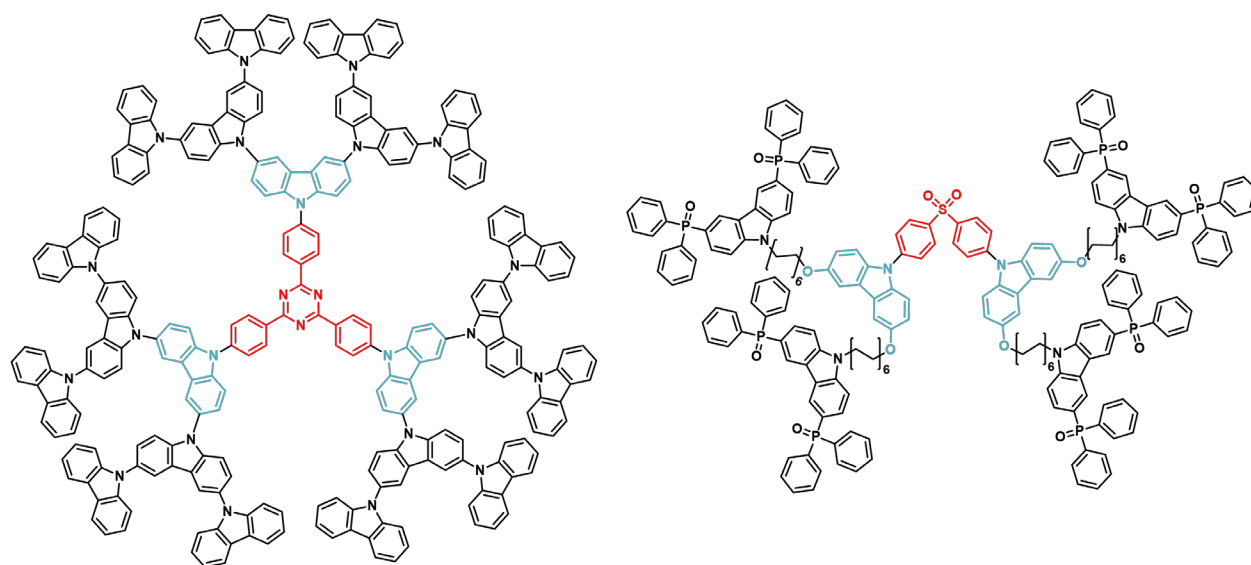


Figure 20. Molecular structures of two types of dendritic TADF emitters based on fully⁹⁸ (left) and partially [102] (right) conjugated dendrons. The acceptor and donor units are indicated in red and blue, respectively.

the conjugated dendrons [102, 103]. For a more extensive overview of dendritic TADF materials, several reviews can be consulted [74, 76, 104].

For polymer-based TADF OLEDs, several design strategies are available. First, a distinction between non-conjugated and conjugated backbones can be made (Figure 21). Within the polymers with a conjugated backbone, a second division can be made between polymers in which the backbone consists of alternating D and A units (Figure 21b) and polymers in which the backbone consists of (a single or alternating) D units to which the A unit is grafted as a side chain (Figure 21c). The opposite case in which the backbone is constructed of A units is less straightforward as the reactive sites used for polymerization are the same as those used for the construction of the D-A bond. In non-conjugated polymers (Figure 21), the backbone is formed by polymerization of styrene-like [105-108] or acrylate [109] monomers via controlled free-radical polymerization techniques or by functionalized norbornenes [110] via ring-opening metathesis polymerization (ROMP). A TADF emitter is incorporated in the monomer structure and is copolymerized with another monomer containing a hole-transporting functionality such as carbazole.

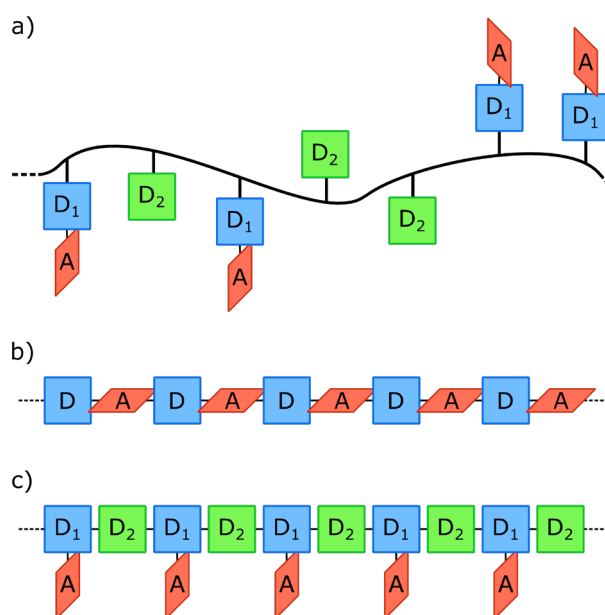


Figure 21. Design motifs for TADF-based polymers. Adapted from *The Chemical Record*, 2019, 19, 1624-1643, with the permission of John Wiley and Sons.

Conjugated D-A alternating copolymers consisting of twisted D-A units suffer from poor charge transport along the polymer backbone and therefore these polymers need to have an additional charge-transporting host material in which they are imbedded [111]. To reduce self-quenching and to improve the charge carrier mobility, either a non-conjugated spacer can be incorporated between the various D-A

blocks [112] or the D-A TADF emitters were copolymerized with an additional donor unit which acts as a kind of host material [113]. The most employed strategy is copolymerization of multiple, typically one or two, donor units to one of which an acceptor unit is grafted. The other donor unit in the backbone then acts as a kind of host material, improving charge carrier mobility, and is sometimes functionalized to further improve these properties [74, 76, 111, 114-120].

4. Alternative triplet upconversion strategies

4.1. Triplet-triplet annihilation

Since the discovery of TTA, sometimes called triplet fusion (TF), in 1962 by Parker *et al.* [40] (*vide supra*), it is well known as an upconversion mechanism to form singlet excited states. Proceeding via a Dexter energy transfer mechanism (Figure 22), two molecules with excited triplet configurations need to be in close proximity to form one de-excited molecule and one molecule with an excited singlet configuration. As twice the triplet excitation energy is generally larger than the first singlet excitation energy, it can occur that a higher singlet state (S_n) is formed first, after which IC takes place to arrive at the first excited singlet state (S_1), followed by fluorescence (Figure 22). In time-resolved emission spectroscopy, TTA can be distinguished from other types of delayed

emission by varying the laser power and looking at the delayed emission intensity. When the emission intensity increases linearly with a slope of 2 in a log-log plot versus the laser energy, the emission is coming from TTA, whereas a slope of 1 indicates TADF. This is because the likelihood of two triplet excitons being in close proximity increases with high exciton formation. The TTA mechanism is especially prevalent under electrical excitation where, according to spin statistics, 75% of the excitons are formed in the triplet configuration. However, because two triplet states are converted to one singlet state, the IQE of a resulting OLED can only be 62.5% (initial 25% plus half of the triplet states formed), which is significantly lower than the 100% IQE achievable via phosphorescent or TADF-based OLEDs. Nevertheless, TTA has played a significant role in the development of early OLED devices, and to this day remains an attractive prospect for the fabrication of blue-emitting OLEDs. As early fluorescent devices were only able to effectively use 25% of the formed excitons, the device EQEs were theoretically limited to ~5%, taking into account a device outcoupling efficiency of approximately 20%. However, reports of fluorescent OLEDs with EQEs above the theoretical limit of 5% do exist. While other effects such as increased device outcoupling or improved selectivity for the generation of singlet excitons upon electrical excitation are possible, they are unable to account for the large increase in EQE. In 1998, Kido and Iizumi were

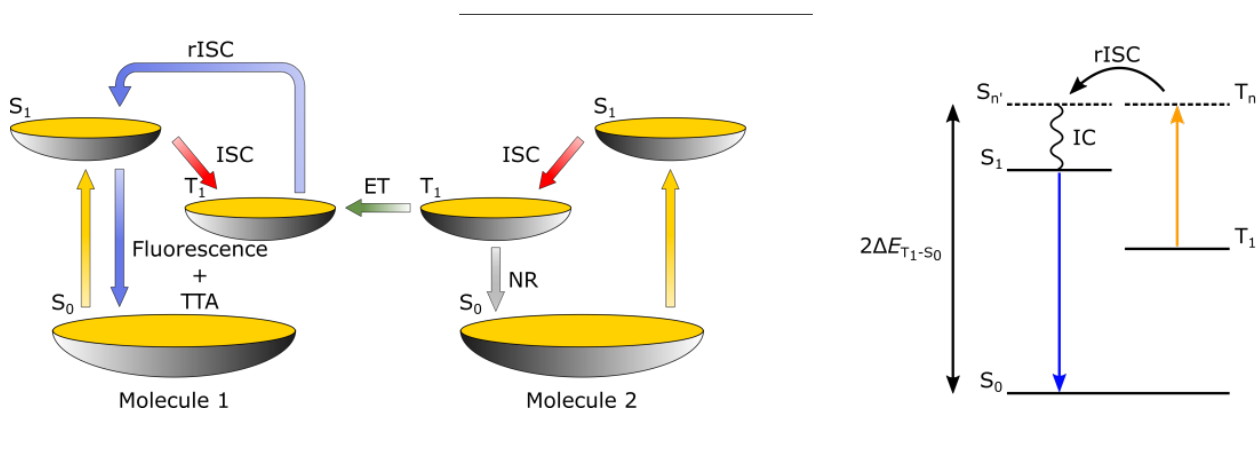


Figure 22. Schematic overview of Dexter energy transfer in TTA (left) and how it leads to singlet emission by combining 2 excited triplet states (right). ET = energy transfer, NR = non-radiative relaxation.

the first to suggest TTA as the plausible pathway for their record EQE (at the time) of 7.1% [121]. In 1999 and 2003, Partee *et al.* [122] and Sinha and Monkman [123] reported TTA as an efficiency boosting mechanism in PPV and MEH-PPV based OLEDs, respectively. In many other reports throughout the beginning of the 21st century, TTA is the likely candidate to explain EQEs above 5% for traditional fluorescent OLEDs. However, with the advent of phosphorescent and TADF-based OLEDs, research in this area has slowed down, with the exception of blue-emitting materials [117-119]. Despite the promise and achievement of higher EQEs for blue-emitting OLEDs using either phosphorescent iridium or TADF-based emitters, they both lack in device lifetime, while color purity is also an issue for the latter [124-126]. Poor electrochemical stability as a result of the fluorine substituents typically used for blue Ir-complexes (Figure 10) and instability of the metal-ligand bonds due to the high triplet energy (>2.7 eV) causes the blue phosphorescent OLEDs to have poor operation lifetimes [126]. While TADF emitters do not suffer from the same metal-ligand related issues, the inherently high triplet energy still causes deterioration of the emitter, with relatively short lifetimes as a result [126]. Furthermore, the CT character of the emission leads to broad emission peaks, affording inferior color purity with respect to the phosphorescent or fluorescent competitors. Blue fluorescent emitters suffer less from these instability issues due to their simpler molecular structures and as such are only hindered by the maximal attainable IQE of 25%. An upconversion mechanism such as TTA is able to boost this to 62.5% and hence can make blue emitters based on TTA viable, as apparent in recent literature [127-129].

4.2. Hybridized local and charge-transfer states

Proposed in 2013 by Ma and co-workers, hybridized local and charge-transfer (HLCT) poses an alternative but similar mechanism to that of TADF (Figure 23) [130]. The HLCT mechanism relies on intersystem crossing between an upper excited triplet state (T_n , $n > 1$) and an excited singlet state (S_n , $n > 0$). HLCT emitters rely on significant LE character in their first excited singlet

state to ensure efficient coupling to the singlet ground state for a high PLQY. Two upper excited states of singlet and triplet multiplicity have to be in close energetic proximity for (r)ISC to occur. The lowest excited triplet state T_1 , typically of LE nature, has to be significantly below T_2 , typically of CT nature, and S_1 to reduce IC from T_2 to T_1 and to prevent TADF from happening from T_1 as large energy gaps reduce the coupling between the various states. ISC is enhanced when the upper states show hybrid LE/CT character [131], which circumvents El-Sayed's rule, but this is not a prerequisite for the HLCT mechanism to occur. Time-resolved emission measurements show that these emitters only have a single lifetime, instead of two as for TADF, indicating a k_{rISC} larger than k_{pF} . The HLCT mechanism thus indirectly increases the amount of excitons in the singlet configuration beyond the statistical 25%, while HLCT materials act as regular fluorescent emitters beyond the initial rISC step. To obtain excited states with hybrid LE/CT character, twisted D-A structures are designed (Figure 23) and (TD)DFT calculations are performed to assess the character and the position of the upper excited states as these are difficult to determine experimentally.

IC is the favored transition according to Kasha's rule (*vide supra*) and the HLCT rISC mechanism is therefore not as efficient as the (r)ISC pathways of TADF can be. This means a significant portion of the 75% formed triplet excitons will still decay non-radiatively to T_1 (k_{IC}), where they are effectively trapped until they can further decay non-radiatively to the ground state (k_{nr}^{T}). As a result, EQEs using this approach have only been around 10% [132, 133]. Because of its heavy reliance on quantum chemical calculations, lack of structure-property relationships that can be deduced and non-ideal working conditions, the HLCT mechanism is currently of less interest to obtain high-efficiency OLEDs.

5. TADF or TTA-sensitized fluorescence

Before the discovery of the multi-resonance DABNA emitters (*vide supra*), researchers were already looking for ways to decrease the emission

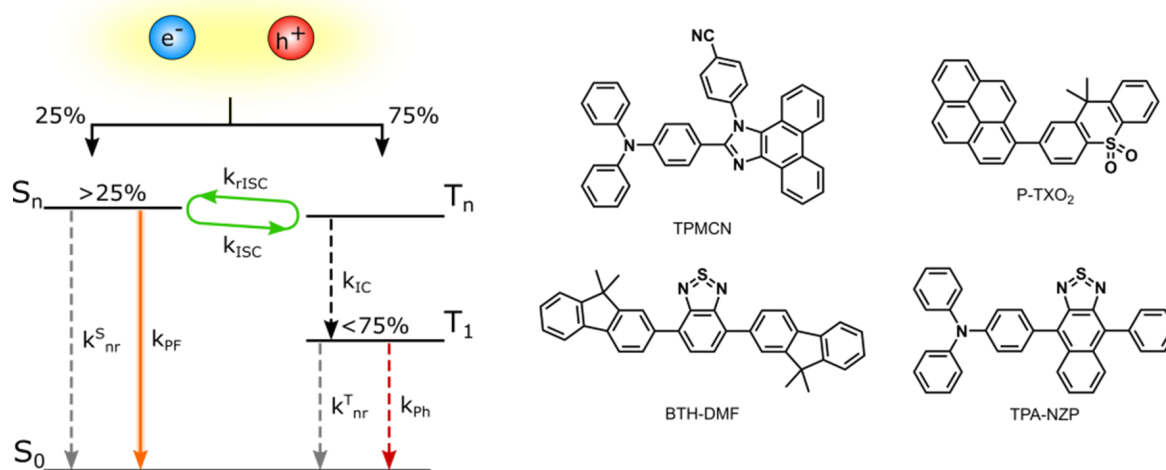


Figure 23. Simplified schematic overview of the HLCT triplet upconversion mechanism (left) and chemical structures of some highly efficient HLCT emitters: TPMCN [128], P-TXO₂ [131], BTH-DMF [132] and TPA-NZP [130] (right).

width (to achieve higher color purity) and to improve on device stability. In 2014, an alternative OLED design strategy was reported by combining a TADF emitter with a fluorescent emitter doped in a wide-energy-gap host material in the active layer [134]. This strategy is sometimes called generation 3.5 and was termed hyperfluorescenceTM by Kyulux. The TADF emitter is used as an assistant dopant and is chosen as such that its singlet and triplet energy levels are above those of the fluorescent emitter. Subsequently, exciton formation occurs on the assistant dopant and the triplet excitons are converted to the assistant dopant singlet state through rISC. Förster resonance energy transfer (FRET) allows transfer of the singlet excitons from the TADF assistant dopant to the narrow-width, high-PLQY fluorescence emitter (Figure 24). The positioning of the energy levels of the assistant dopant and the fluorescent dopant are crucial and careful tuning is necessary to allow exciton formation solely on the assistant dopant and efficient energy transfer to the fluorescent dopant [135, 136]. To help achieving this, the assistant dopant is typically doped at 10–50 wt%, whereas the fluorescent emitter is doped at very low concentrations (below 5 wt%). This sensitized approach allows optimal usage of excitons (up to 100% IQE) in combination with the narrow emission width, high PLQY and large k_{PF} of the fluorescent emitter [135]. However, because an additional energy transfer step is required for the

fluorescent emitter, the design of these systems requires even more tuning of the energy levels of the OLED layers and active materials [136].

While the advent of TADF sparked new hope for stable blue-emitting materials, large roll-off of the device efficiencies remained, even for blue TADF materials. The main problem is the inherently high-lying triplet state, a property that all blue phosphorescent and TADF materials share, which leads to rapid degradation of the OLED devices [126, 137–139]. Even with the TADF-sensitized fluorescent OLED approach, the concentration of the TADF dopant is sufficiently high to have a rapid decrease in device efficiency. Alternatively, TTA molecules can be used for triplet upconversion in combination with a fluorescent emitter via the same mechanism [140]. The benefit of TTA molecules is the presence of low-lying triplet states ($S_1 \approx 2 \times T_1$), which give the TTA molecules greater stability [141]. The downside of the TTA mechanism is the limited IQE of 62.5 % which can be obtained when all triplet excitons are upconverted (*vide supra*). These TTA-sensitized fluorescent OLEDs will give lower overall device efficiencies but improved device lifetimes over their TADF counterparts. It is then up to industry to determine how to best manage these advantages and disadvantages in order for the development of OLEDs to move forward.

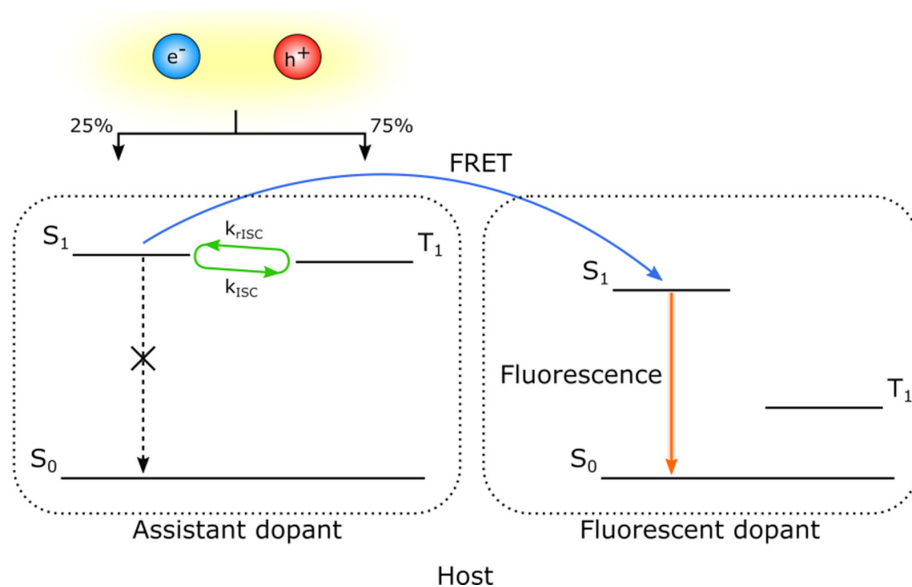


Figure 24. Schematic overview of the TADF-sensitized fluorescent OLED design.

6. Rational design of TADF emitters through a joint synthetic and computational chemistry approach

In the past couple of years, the author of this overview article has collaborated on the tailored design of novel TADF emitters by combining quantum-chemical (TDDFT), synthetic, and photophysical analysis efforts. In the final section, a short summary of the most important results obtained so far is given.

The use of TDDFT calculations to predict the excited state properties of conjugated materials has become commonplace in organic electronics research. To better understand how different exchange-correlation functionals (XCFs) influence the obtained excited state properties of potential TADF materials, a series of 10 prototypical donor-acceptor compounds were subjected to thorough investigation with DFT and TDDFT and their excited state properties such as the excitation energies and oscillator strengths were calculated using 19 different XCFs with various levels of complexity [142]. These values were benchmarked against a high level wavefunction method called resolution-of-the-identity second order approximation coupled-cluster (riCC2). The best performing functional was the long-range corrected LC-BLYP with

a value for ω of 0.17 bohr^{-1} . Application of the Tamm-Dancoff approximation [143] (often used to overcome triplet instabilities) was found to improve the error on the triplet excitation energies with respect to those obtained using riCC2, and resulted in even smaller errors for the singlet-triplet energy splittings.

One of the main research lines in our research groups is to expand on the known pool of donor and acceptor moieties that can be used to construct D-A and D-A-D type emissive materials for 3rd generation OLEDs. To achieve this, other fields of organic electronics, most notably the field of organic photovoltaics (OPVs), serve as an inspiration for new building blocks that have not been applied before in the field of OLEDs. With the help of quantum chemistry methods such as those mentioned before, we are able to rationally design new emitters based on the findings from the calculations. One such donor unit that we have introduced is benzo[1,2-*b*:4,5-*b'*]dithiophene (BDT), a well-known OPV donor unit as it possesses a high electron-donating strength, high planarity and often affords a high charge carrier mobility. Unfortunately, conventional coupling of this unit via the α -positions would lead to planar D-A molecules, not likely to show TADF properties. As such, a synthetic pathway to couple the donor and acceptor units via the benzene core

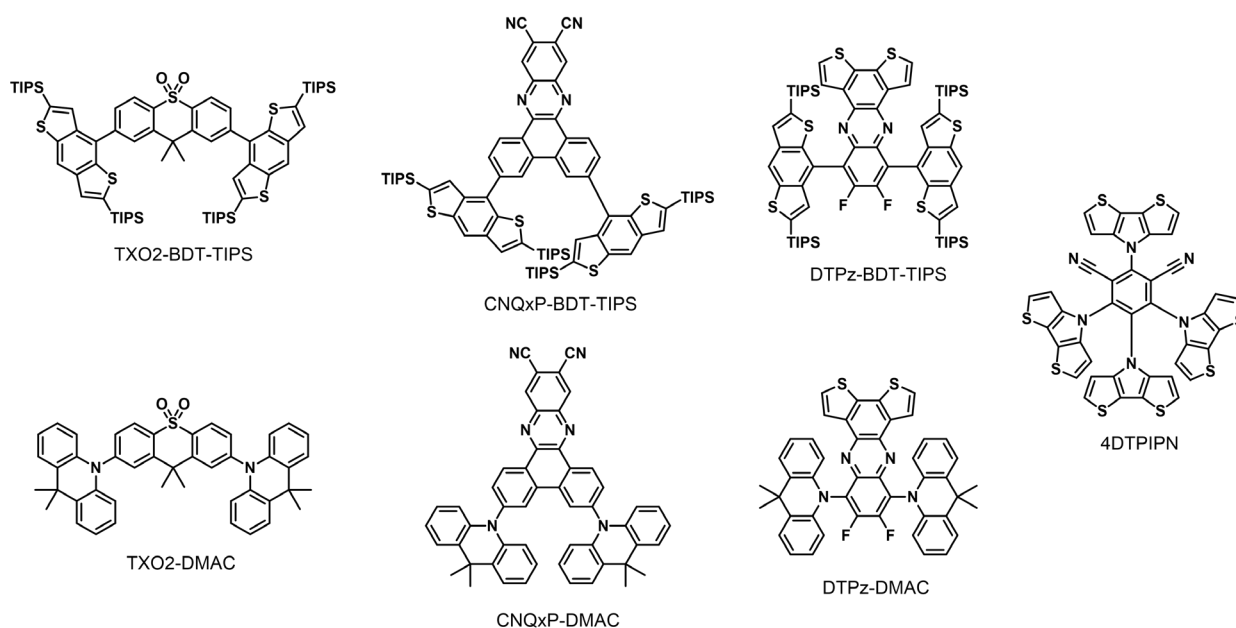


Figure 25. Molecular structures of the BDT-TIPS, DMAC and DTP-based compounds.

of BDT had to be developed. The BDT unit was coupled to 3 different acceptors: 9,9-dimethyl-9H-thioxanthene-10,10-dioxide (TXO2) [144], dibenzo[*a,c*]phenazine-11,12-dicarbonitrile (CNQxP) [144] and difluorodithieno[3,2-*a*:2',3'-*c*]phenazine (DTPz) (Figure 25) [145]. To compare their properties, the 9,9-dimethyl-9,10-dihydroacridine (DMAC) analogues were designed. On top of that, the DTPz unit is also a new strongly electron-accepting unit which has been used for the construction of TADF materials for the first time [145]. Photophysical characterization in zeonex films showed prompt and delayed emission for all 6 compounds (Figure 26). However, their nature differed. The DMAC-containing compounds showed TADF, whereas the BDT-based compounds showed room temperature phosphorescence (RTP) when TXO2 and DTPz were chosen as the acceptor and TADF when CNQxP was chosen as the acceptor. The RTP behavior of TXO2-BDT-TIPS (Figure 26a) is unusual and was attributed to the presence of multiple sulfur atoms in the BDT unit. Therefore, we investigated the BDT-TIPS donor unit by itself and found similar RTP behavior in zeonex film. The RTP emission of DTPz-BDT-TIPS differed from that of TXO2-BDT-TIPS and was attributed to phosphorescence coming from the DTPz core instead. CNQxP-BDT-TIPS and CNQxP-DMAC showed long-lived TADF with some TTA at

very long emission times. The main difference between TXO2-BDT-TIPS and CNQxP-BDT-TIPS is the acceptor strength. While the localized triplet state of the BDT-TIPS group, responsible for the phosphorescent behavior, is below the CT states for TXO2-BDT-TIPS, this is not the case for CNQxP-BDT-TIPS. The smaller experimental singlet-triplet energy splitting also resulted in the possibility of rISC to occur for CNQxP-BDT-TIPS, whereas this is not possible for TXO2-BDT-TIPS.

In addition to the introduction of the BDT and DTPz units, 4H-dithieno[3,2-*b*:2',3'-*d*]pyrrole (DTP; Figure 26) was chosen as the donor unit to replace 9H-carbazole in 4CzIPN (Figure 15) [146], originally reported by Adachi and coworkers [46]. It was further studied by Etherington *et al.* [147] and was found to show extensive dimer formation in doped OLED films originating from interactions between the carbazole units of different molecules. Dimer emission is undesired in OLED devices as it compromises the color purity. Synthesis of the DTP unit via a carbamate intermediate allows the free-base DTP to be obtained after which it can be used in nucleophilic aromatic substitution or Buchwald-Hartwig type reactions to form D-A or D-A-D type materials. The former was applied to construct 4DTP-IPN, using

similar reaction conditions as for the synthesis of 4CzIPN. 4DTP-IPN showed red-shifted emission with respect to that of 4CzIPN and exhibited TADF properties in a variety of films and at different concentrations. Unfortunately, instead of removing the dimerization, the DTP

unit enhances aggregation and it persists even at 0.01 wt% doping in polymer and small molecule films. While this enhances the color purity of the emission, the PLQY drops because of the aggregational quenching and this is obviously not desired for OLED applications.

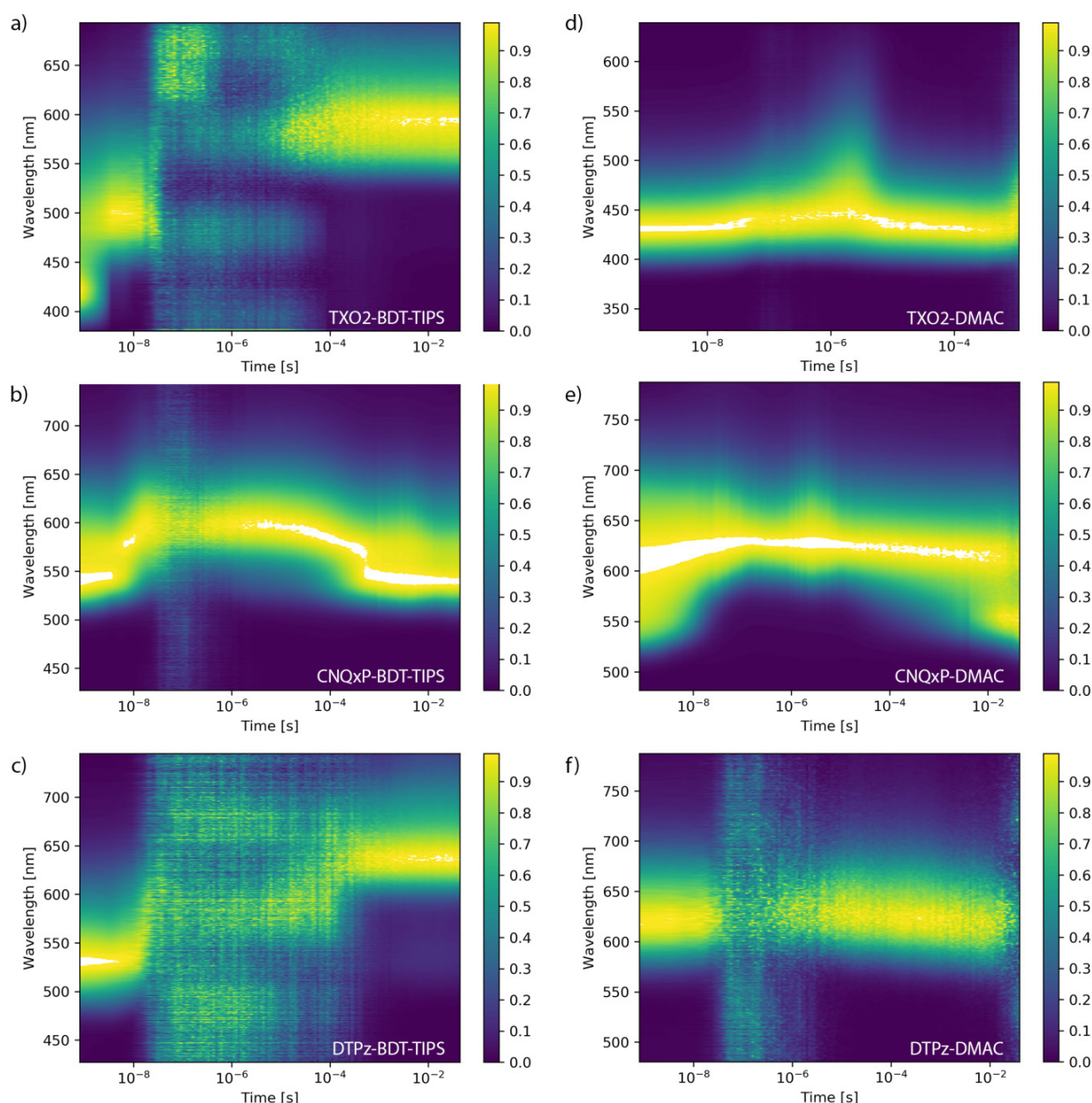


Figure 26: Normalized time-resolved emission spectra for BDT-TIPS-based compounds (left) and DMAC-based compounds (right) in zeonex at room temperature. The colour intensity shows the emission wavelength at various emission times during the decay. When the delayed emission appears at the same wavelength as prompt emission, triplet upconversion mechanisms such as TADF and TTA are at play. For TXO2-BDT-TIPS and DTPz-BDT-TIPS, the delayed emission corresponds to the triplet emission at 80K. Adapted from *Dyes and Pigments*, 2021, 186, 109022 and *Dyes and Pigments*, 2021, 190, 109301, with the permission of Elsevier [143, 144].

7. Conclusions

In the presented work, a historic overview of some crucial discoveries in the field of organic light-emitting diodes is given. Special attention is devoted to the principle of thermally activated delayed fluorescence or TADF for triplet upconversion as this is the most researched sub-topic in the field at present. While device

stability and lifetime for blue emitters is still an issue, solutions are presented by the TADF and TTA-sensitized fluorescent OLEDs and these technologies could bring additional relevance to the field of OLEDs in the years to come. The interplay of quantum-chemical calculations, synthesis efforts and detailed (time-resolved) photophysical analysis seems crucial to foster further progress.

References

- [1] G. Destriau, *J. Chim. Phys.*, 1936, 33, 587-625.
- [2] A. Bernanose, M. Comte and P. Vouaux, *J. Chim. Phys.*, 1953, 50, 64-68.
- [3] M. Pope, H. P. Kallmann and P. Magnante, *The Journal of Chemical Physics*, 1963, 38, 2042-2043.
- [4] C. W. Tang and S. A. VanSlyke, *Applied Physics Letters*, 1987, 51, 913-915.
- [5] C. W. Tang, S. A. VanSlyke and C. H. Chen, *Journal of Applied Physics*, 1989, 65, 3610-3616.
- [6] C. Adachi, S. Tokito, T. Tsutsui and S. Saito, *Japanese Journal of Applied Physics*, 1988, 27, L713-L715.
- [7] C. Adachi, S. Tokito, T. Tsutsui and S. Saito, *Japanese Journal of Applied Physics*, 1988, 27, L269-L271.
- [8] C. Adachi, T. Tsutsui and S. Saito, *Applied Physics Letters*, 1989, 55, 1489-1491.
- [9] J. H. Burroughes, D. D. C. Bradley, A. R. Brown, R. N. Marks, K. Mackay, R. H. Friend, P. L. Burns and A. B. Holmes, *Nature*, 1990, 347, 539-541.
- [10] Y. Ohmori, M. Uchida, K. Muro and K. Yoshino, *Japanese Journal of Applied Physics*, 1991, 30, L1938-L1940.
- [11] Y. Ohmori, M. Uchida, K. Muro and K. Yoshino, *Japanese Journal of Applied Physics*, 1991, 30, L1941-L1943.
- [12] G. Grem, G. Leditzky, B. Ullrich and G. Leising, *Advanced Materials*, 1992, 4, 36-37.
- [13] D. Braun and A. J. Heeger, *Applied Physics Letters*, 1991, 58, 1982-1984.
- [14] Merck, <https://www.merckgroup.com/business-specifics/performance-materials/Optoelectronics/global/Datasheet-Livilux-PDY-132-Super-Yellow-EN.pdf>.
- [15] J. K. Borchardt, *Materials Today*, 2004, 7, 42-46.
- [16] P.-W. Wang, Y.-J. Liu, C. Devadoss, P. Bharathi and J. S. Moore, *Advanced Materials*, 1996, 8, 237-241.
- [17] J. N. G. Pillow, M. Halim, J. M. Lupton, P. L. Burn and I. D. W. Samuel, *Macromolecules*, 1999, 32, 5985-5993.
- [18] C. C. Kwok and M. S. Wong, *Macromolecules*, 2001, 34, 6821-6830.
- [19] Y. Zou, J. Zou, T. Ye, H. Li, C. Yang, H. Wu, D. Ma, J. Qin and Y. Cao, *Advanced Functional Materials*, 2013, 23, 1781-1788.
- [20] S. R. Forrest, D. D. C. Bradley and M. E. Thompson, *Advanced Materials*, 2003, 15, 1043-1048.
- [21] W. Brütting, J. Frischauf, T. D. Schmidt, B. J. Scholz and C. Mayr, *physica status solidi (a)*, 2013, 210, 44-65.
- [22] J. Kido, K. Nagai and Y. Ohashi, *Chemistry Letters*, 1990, 19, 657-660.
- [23] J. Kido, K. Nagai and Y. Okamoto, *Journal of Alloys and Compounds*, 1993, 192, 30-33.
- [24] M. A. Baldo, D. F. O'Brien, Y. You, A. Shoustikov, S. Sibley, M. E. Thompson and S. R. Forrest, *Nature*, 1998, 395, 151-154.
- [25] R. C. Kwong, S. Sibley, T. Dubovoy, M. Baldo, S. R. Forrest and M. E. Thompson, *Chemistry of Materials*, 1999, 11, 3709-3713.
- [26] A. A. Shoustikov, Y. Yujian and M. E. Thompson, *IEEE Journal of Selected Topics in Quantum Electronics*, 1998, 4, 3-13.
- [27] S.-Y. Lu, S. Mukhopadhyay, R. Froese and P. M. Zimmerman, *Journal of Chemical Information and Modeling*, 2018, 58, 2440-2449.
- [28] M. Ikai, S. Tokito, Y. Sakamoto, T. Suzuki and Y. Taga, *Applied Physics Letters*, 2001, 79, 156-158.
- [29] C. Adachi, R. C. Kwong, P. Djurovich, V. Adamovich, M. A. Baldo, M. E. Thompson and S. R. Forrest, *Applied Physics Letters*, 2001, 79, 2082-2084.
- [30] C. Adachi, M. A. Baldo, S. R. Forrest, S. Lamansky, M. E. Thompson and R. C. Kwong, *Applied Physics Letters*, 2001, 78, 1622-1624.
- [31] A. Tsuboyama, H. Iwawaki, M. Furugori, T. Mukaide, J. Kamatani, S. Igawa, T. Moriyama, S. Miura, T. Takiguchi, S. Okada, M. Hoshino and K. Ueno, *Journal of the American Chemical Society*, 2003, 125, 12971-12979.
- [32] C. Bizzarri, F. Hundemer, J. Busch and S. Bräse, *Polyhedron*, 2018, 140, 51-66.
- [33] H. Xu, R. Chen, Q. Sun, W. Lai, Q. Su, W. Huang and X. Liu, *Chemical Society Reviews*, 2014, 43, 3259-3302.
- [34] J. Hyocheol, S. Hwangyu, L. Jaehyun, K. Beomjin, P. Young-II, Y. Kyoung Soo, A. Byeong-Kwan and P. Jongwook, *Journal of Photonics for Energy*, 2015, 5, 1-23.
- [35] J.-H. Jou, S. Kumar, A. Agrawal, T.-H. Li and S. Sahoo, *Journal of Materials Chemistry C*, 2015, 3, 2974-3002.
- [36] Q. Wei, N. Fei, A. Islam, T. Lei, L. Hong, R. Peng, X. Fan, L. Chen, P. Gao and Z. Ge, *Advanced Optical Materials*, 2018, 6, 1800512.
- [37] R. Delorme and F. Perrin, *J. Phys. Radium*, 1929, 10, 177-186.
- [38] G. N. Lewis, D. Lipkin and T. T. Magel, *Journal of the American Chemical Society*, 1941, 63, 3005-3018.
- [39] C. A. Parker and C. G. Hatchard, *Transactions of the Faraday Society*, 1961, 57, 1894-1904.
- [40] C. A. Parker, C. G. Hatchard and E. J. Bowen, *Proceedings of the Royal Society of London. Series A. Mathematical and Physical Sciences*, 1962, 269, 574-584.
- [41] Y. Onoue, K. Hiraki and Y. Nishikawa, *Bulletin of the Chemical Society of Japan*, 1981, 54, 2633-2635.
- [42] Y. Nishikawa, K. Hiraki, Y. Onoue, K. Nishikawa, Y. Yoshitake and T. Shigematsu, *Bunseki Kagaku*, 1983, 32, E115-E122.
- [43] M. N. Berberan-Santos and J. M. M. Garcia, *Journal of the American Chemical Society*, 1996, 118, 9391-9394.
- [44] M. W. Wolf, K. D. Legg, R. E. Brown, L. A. Singer and J. H. Parks, *Journal of the American Chemical Society*, 1975, 97, 4490-4497.

- [45] A. Maciejewski, M. Szymanski and R. P. Steer, *The Journal of Physical Chemistry*, 1986, 90, 6314-6318.
- [46] A. Endo, M. Ogasawara, A. Takahashi, D. Yokoyama, Y. Kato and C. Adachi, *Adv Mater*, 2009, 21, 4802-4806.
- [47] A. Endo, K. Sato, K. Yoshimura, T. Kai, A. Kawada, H. Miyazaki and C. Adachi, *Applied Physics Letters*, 2011, 98, 083302.
- [48] G. Méhes, H. Nomura, Q. Zhang, T. Nakagawa and C. Adachi, *Angewandte Chemie International Edition*, 2012, 51, 11311-11315.
- [49] T. Nakagawa, S.-Y. Ku, K.-T. Wong and C. Adachi, *Chemical Communications*, 2012, 48, 9580-9582.
- [50] H. Tanaka, K. Shizu, H. Miyazaki and C. Adachi, *Chemical Communications*, 2012, 48, 11392-11394.
- [51] H. Uoyama, K. Goushi, K. Shizu, H. Nomura and C. Adachi, *Nature*, 2012, 492, 234-238.
- [52] S. Youn Lee, T. Yasuda, H. Nomura and C. Adachi, *Applied Physics Letters*, 2012, 101, 093306.
- [53] Q. Zhang, J. Li, K. Shizu, S. Huang, S. Hirata, H. Miyazaki and C. Adachi, *Journal of the American Chemical Society*, 2012, 134, 14706-14709.
- [54] J. Lee, K. Shizu, H. Tanaka, H. Nomura, T. Yasuda and C. Adachi, *Journal of Materials Chemistry C*, 2013, 1, 4599-4604.
- [55] K. Nasu, T. Nakagawa, H. Nomura, C.-J. Lin, C.-H. Cheng, M.-R. Tseng, T. Yasuda and C. Adachi, *Chemical Communications*, 2013, 49, 10385-10387.
- [56] H. Tanaka, K. Shizu, H. Nakanotani and C. Adachi, *Chemistry of Materials*, 2013, 25, 3766-3771.
- [57] F. B. Dias, K. N. Bourdakos, V. Jankus, K. C. Moss, K. T. Kamtekar, V. Bhalla, J. Santos, M. R. Bryce and A. P. Monkman, *Advanced Materials*, 2013, 25, 3707-3714.
- [58] M. Kasha, *Discussions of the Faraday Society*, 1950, 9, 14-19.
- [59] T. J. Penfold, F. B. Dias and A. P. Monkman, *Chemical Communications*, 2018, 54, 3926-3935.
- [60] J. Gibson and T. J. Penfold, *Physical Chemistry Chemical Physics*, 2017, 19, 8428-8434.
- [61] W. Che, Y. Xie and Z. Li, *Asian Journal of Organic Chemistry*, 2020, 9, 1262-1276.
- [62] X. Liang, Z.-L. Tu and Y.-X. Zheng, *Chemistry – A European Journal*, 2019, 25, 5623-5642.
- [63] M. A. El Sayed, *The Journal of Chemical Physics*, 1963, 38, 2834-2838.
- [64] M. Baba, *J Phys Chem A*, 2011, 115, 9514-9519.
- [65] T. Ogiwara, Y. Wakikawa and T. Ikoma, *The Journal of Physical Chemistry A*, 2015, 119, 3415-3418.
- [66] J. Gibson, A. P. Monkman and T. J. Penfold, *ChemPhysChem*, 2016, 17, 2956-2961.
- [67] J. S. Ward, R. S. Nobuyasu, A. S. Batsanov, P. Data, A. P. Monkman, F. B. Dias and M. R. Bryce, *Chemical Communications*, 2016, 52, 2612-2615.
- [68] P. L. Santos, J. S. Ward, P. Data, A. S. Batsanov, M. R. Bryce, F. B. Dias and A. P. Monkman, *Journal of Materials Chemistry C*, 2016, 4, 3815-3824.
- [69] X.-K. Chen, S.-F. Zhang, J.-X. Fan and A.-M. Ren, *The Journal of Physical Chemistry C*, 2015, 119, 9728-9733.
- [70] F. B. Dias, J. Santos, D. R. Graves, P. Data, R. S. Nobuyasu, M. A. Fox, A. S. Batsanov, T. Palmeira, M. N. Berberan-Santos, M. R. Bryce and A. P. Monkman, *Advanced Science*, 2016, 3, 1600080.
- [71] C. M. Marian, *The Journal of Physical Chemistry C*, 2016, 120, 3715-3721.
- [72] T. J. Penfold, E. Gindensperger, C. Daniel and C. M. Marian, *Chemical Reviews*, 2018, 118, 6975-7025.
- [73] M. Y. Wong and E. Zysman-Colman, *Advanced Materials*, 2017, 29, 1605444.
- [74] Z. Yang, Z. Mao, Z. Xie, Y. Zhang, S. Liu, J. Zhao, J. Xu, Z. Chi and M. P. Aldred, *Chemical Society Reviews*, 2017, 46, 915-1016.
- [75] T.-T. Bui, F. Goubard, M. Ibrahim-Ouali, D. Gigmes and F. Dumur, *Beilstein Journal of Organic Chemistry*, 2018, 14, 282-308.
- [76] Y. Liu, C. Li, Z. Ren, S. Yan and M. R. Bryce, *Nature Reviews Materials*, 2018, 3, 18020.
- [77] J. Sohn, D. Ko, H. Lee, J. Han, S.-D. Lee and C. Lee, *Organic Electronics*, 2019, 70, 286-291.
- [78] J. U. Kim, I. S. Park, C.-Y. Chan, M. Tanaka, Y. Tsuchiya, H. Nakanotani and C. Adachi, *Nature Communications*, 2020, 11, 1765.
- [79] S. Scholz, D. Kondakov, B. Lüssem and K. Leo, *Chemical Reviews*, 2015, 115, 8449-8503.
- [80] Y. Im, S. Y. Byun, J. H. Kim, D. R. Lee, C. S. Oh, K. S. Yook and J. Y. Lee, *Advanced Functional Materials*, 2017, 27, 1603007.
- [81] H. Lee, D. Karthik, R. Lampande, J. H. Ryu and J. H. Kwon, *Frontiers in Chemistry*, 2020, 8, 373.
- [82] J.-M. Teng, Y.-F. Wang and C.-F. Chen, *Journal of Materials Chemistry C*, 2020, 8, 11340-11353.
- [83] S. S. Kothavale and J. Y. Lee, *Advanced Optical Materials*, 2020, 8, 2000922.
- [84] T. Hatakeyama, K. Shiren, K. Nakajima, S. Nomura, S. Nakatsuka, K. Kinoshita, J. Ni, Y. Ono and T. Ikuta, *Advanced Materials*, 2016, 28, 2777-2781.
- [85] S. H. Han, J. H. Jeong, J. W. Yoo and J. Y. Lee, *Journal of Materials Chemistry C*, 2019, 7, 3082-3089.
- [86] Y. Kondo, K. Yoshiura, S. Kitera, H. Nishi, S. Oda, H. Gotoh, Y. Sasada, M. Yanai and T. Hatakeyama, *Nature Photonics*, 2019, 13, 678-682.
- [87] R. Englman and J. Jortner, *Molecular Physics*, 1970, 18, 145-164.
- [88] M. Bixon, J. Jortner, J. Cortes, H. Heitele and M. E. Michel-Beyerle, *The Journal of Physical Chemistry*, 1994, 98, 7289-7299.
- [89] J. H. Kim, J. H. Yun and J. Y. Lee, *Advanced Optical Materials*, 2018, 6, 1800255.
- [90] Z. Chen, Z. Wu, F. Ni, C. Zhong, W. Zeng, D. Wei, K. An, D. Ma and C. Yang, *Journal of Materials Chemistry C*, 2018, 6, 6543-6548.
- [91] X. Xiong, F. Song, J. Wang, Y. Zhang, Y. Xue, L. Sun, N. Jiang, P. Gao, L. Tian and X. Peng, *Journal of the American Chemical Society*, 2014, 136, 9590-9597.
- [92] W. Hu, L. Guo, L. Bai, X. Miao, Y. Ni, Q. Wang, H. Zhao, M. Xie, L. Li, X. Lu, W. Huang and Q. Fan, *Advanced Healthcare Materials*, 2018, 7, 1800299.
- [93] Z. Zhu, D. Tian, P. Gao, K. Wang, Y. Li, X. Shu, J. Zhu and Q. Zhao, *Journal of the American Chemical Society*, 2018, 140, 17484-17491.
- [94] F. Ni, Z. Zhu, X. Tong, W. Zeng, K. An, D. Wei, S. Gong, Q. Zhao, X. Zhou and C. Yang, *Advanced Science*, 2019, 6, 1801729.
- [95] C. I. C. Crucho, J. Avó, A. M. Diniz, S. N. Pinto, J. Barbosa, P. O. Smith, M. N. Berberan-Santos, L.-O. Pålsson and F. B. Dias, *Frontiers in Chemistry*, 2020, 8, 404.
- [96] S. Xu, Q. Zhang, X. Han, Y. Wang, X. Wang, M. Nazare, J.-D. Jiang and H.-Y. Hu, *ACS Sensors*, 2020, 5, 1650-1656.
- [97] W. Zhao, H. Wei, F. Liu and C. Ran, *Photodiagnosis and Photodynamic Therapy*, 2020, 30, 101744.

- [98] K. Albrecht, K. Matsuoka, K. Fujita and K. Yamamoto, *Angewandte Chemie International Edition*, 2015, 54, 5677-5682.
- [99] Y. Li, G. Xie, S. Gong, K. Wu and C. Yang, *Chemical Science*, 2016, 7, 5441-5447.
- [100] J. Luo, S. Gong, Y. Gu, T. Chen, Y. Li, C. Zhong, G. Xie and C. Yang, *Journal of Materials Chemistry C*, 2016, 4, 2442-2446.
- [101] K. Albrecht, K. Matsuoka, D. Yokoyama, Y. Sakai, A. Nakayama, K. Fujita and K. Yamamoto, *Chemical Communications*, 2017, 53, 2439-2442.
- [102] X. Ban, W. Jiang, K. Sun, B. Lin and Y. Sun, *ACS Applied Materials & Interfaces*, 2017, 9, 7339-7346.
- [103] K. Sun, Y. Sun, T. Huang, J. Luo, W. Jiang and Y. Sun, *Organic Electronics*, 2017, 42, 123-130.
- [104] J.-L. Wu, Y.-T. Lee, C.-T. Chen and C.-T. Chen, *Journal of the Chinese Chemical Society*, 2018, 65, 87-106.
- [105] Z. Ren, R. S. Nobuyasu, F. B. Dias, A. P. Monkman, S. Yan and M. R. Bryce, *Macromolecules*, 2016, 49, 5452-5460.
- [106] C. Li, Y. Wang, D. Sun, H. Li, X. Sun, D. Ma, Z. Ren and S. Yan, *ACS Applied Materials & Interfaces*, 2018, 10, 5731-5739.
- [107] C. Li, Z. Ren, X. Sun, H. Li and S. Yan, *Macromolecules*, 2019, 52, 2296-2303.
- [108] J. Hu, Q. Li, S. Shao, L. Wang, X. Jing and F. Wang, *Advanced Optical Materials*, 2020, 8, 1902100.
- [109] C. J. Christopherson, D. M. Mayder, J. Poisson, N. R. Paisley, C. M. Tonge and Z. M. Hudson, *ACS Applied Materials & Interfaces*, 2020, 12, 20000-20011.
- [110] X. Zeng, J. Luo, T. Zhou, T. Chen, X. Zhou, K. Wu, Y. Zou, G. Xie, S. Gong and C. Yang, *Macromolecules*, 2018, 51, 1598-1604.
- [111] B. Zhang and Y. Cheng, *The Chemical Record*, 2019, 19, 1624-1643.
- [112] A. E. Nikolaenko, M. Cass, F. Bourcet, D. Mohamad and M. Roberts, *Advanced Materials*, 2015, 27, 7236-7240.
- [113] S. Y. Lee, T. Yasuda, H. Komiyama, J. Lee and C. Adachi, *Advanced Materials*, 2016, 28, 4019-4024.
- [114] D. M. E. Freeman, A. J. Musser, J. M. Frost, H. L. Stern, A. K. Forster, K. J. Fallon, A. G. Rapisdi, F. Cacialli, I. McCulloch, T. M. Clarke, R. H. Friend and H. Bronstein, *Journal of the American Chemical Society*, 2017, 139, 11073-11080.
- [115] Q. Wei, P. Kleine, Y. Karpov, X. Qiu, H. Komber, K. Sahre, A. Kiriy, R. Lygaitis, S. Lenk, S. Reineke and B. Voit, *Advanced Functional Materials*, 2017, 27, 1605051.
- [116] Y. Liu, Y. Wang, C. Li, Z. Ren, D. Ma and S. Yan, *Macromolecules*, 2018, 51, 4615-4623.
- [117] Y. Wang, Y. Zhu, X. Lin, Y. Yang, B. Zhang, H. Zhan, Z. Xie and Y. Cheng, *Journal of Materials Chemistry C*, 2018, 6, 568-574.
- [118] Y. Liu, G. Xie, Z. Ren and S. Yan, *ACS Applied Polymer Materials*, 2019, 1, 2204-2212.
- [119] Y. Yang, K. Li, C. Wang, H. Zhan and Y. Cheng, *Chemistry – An Asian Journal*, 2019, 14, 574-581.
- [120] Y. Liu, L. Hua, S. Yan and Z. Ren, *Nano Energy*, 2020, 73, 104800.
- [121] J. Kido and Y. Iizumi, *Applied Physics Letters*, 1998, 73, 2721-2723.
- [122] J. Partee, E. L. Frankevich, B. Uhlhorn, J. Shinar, Y. Ding and T. J. Barton, *Physical Review Letters*, 1999, 82, 3673-3676.
- [123] S. Sinha and A. P. Monkman, *Applied Physics Letters*, 2003, 82, 4651-4653.
- [124] A. P. Monkman, *ISRN Materials Science*, 2013, 2013, 670130.
- [125] D. Y. Kondakov, *Philosophical Transactions of the Royal Society A: Mathematical, Physical and Engineering Sciences*, 2015, 373, 20140321.
- [126] J.-H. Lee, C.-H. Chen, P.-H. Lee, H.-Y. Lin, M.-k. Leung, T.-L. Chiu and C.-F. Lin, *Journal of Materials Chemistry C*, 2019, 7, 5874-5888.
- [127] N. A. Kukhta, T. Matulaitis, D. Volyniuk, K. Ivaniuk, P. Turyk, P. Stakhira, J. V. Grazulevicius and A. P. Monkman, *The Journal of Physical Chemistry Letters*, 2017, 8, 6199-6205.
- [128] Y. Takita, K. Takeda, N. Hashimoto, S. Nomura, T. Suzuki, H. Nakashima, S. Uesaka, S. Seo and S. Yamazaki, *Journal of the Society for Information Display*, 2018, 26, 55-63.
- [129] H. W. Bae, G. W. Kim, R. Lampande, J. H. Park, I. J. Ko, H. J. Yu, C. Y. Lee and J. H. Kwon, *Organic Electronics*, 2019, 70, 1-6.
- [130] S. Zhang, W. Li, L. Yao, Y. Pan, F. Shen, R. Xiao, B. Yang and Y. Ma, *Chemical Communications*, 2013, 49, 11302-11304.
- [131] W. Li, Y. Pan, R. Xiao, Q. Peng, S. Zhang, D. Ma, F. Li, F. Shen, Y. Wang, B. Yang and Y. Ma, *Advanced Functional Materials*, 2014, 24, 1609-1614.
- [132] C. Fu, S. Luo, Z. Li, X. Ai, Z. Pang, C. Li, K. Chen, L. Zhou, F. Li, Y. Huang and Z. Lu, *Chemical Communications*, 2019, 55, 6317-6320.
- [133] J. Liu, Z. Li, T. Hu, X. Wei, R. Wang, X. Hu, Y. Liu, Y. Yi, Y. Yamada-Takamura, Y. Wang and P. Wang, *Advanced Optical Materials*, 2019, 7, 1801190.
- [134] H. Nakanotani, T. Higuchi, T. Furukawa, K. Masui, K. Morimoto, M. Numata, H. Tanaka, Y. Sagara, T. Yasuda and C. Adachi, *Nature Communications*, 2014, 5, 4016.
- [135] S. Y. Byeon, D. R. Lee, K. S. Yook and J. Y. Lee, *Advanced Materials*, 2019, 31, 1803714.
- [136] M. Cai, D. Zhang and L. Duan, *The Chemical Record*, 2019, 19, 1611-1623.
- [137] S. R. Forrest, *Philosophical Transactions of the Royal Society A: Mathematical, Physical and Engineering Sciences*, 2015, 373, 20140320.
- [138] L.-S. Cui, Y.-L. Deng, D. P.-K. Tsang, Z.-Q. Jiang, Q. Zhang, L.-S. Liao and C. Adachi, *Advanced Materials*, 2016, 28, 7620-7625.
- [139] A. S. D. Sandanayaka, T. Matsushima and C. Adachi, *The Journal of Physical Chemistry C*, 2015, 119, 23845-23851.
- [140] Z. Xu, B. Z. Tang, Y. Wang and D. Ma, *Journal of Materials Chemistry C*, 2020, 8, 2614-2642.
- [141] C.-J. Chiang, A. Kimyonok, M. K. Etherington, G. C. Griffiths, V. Jankus, F. Turksoy and A. P. Monkman, *Advanced Functional Materials*, 2013, 23, 739-746.
- [142] T. Cardeynaels, S. Paredis, J. Deckers, S. Brebels, D. Vanderzande, W. Maes and B. Champagne, *Phys Chem Chem Phys*, 2020, 22, 16387-16399.
- [143] S. Hirata, M. Head-Gordon, *Chem. Phys. Lett.*, 1999, 314, 291-299.
- [144] T. Cardeynaels, S. Paredis, A. Danos, D. Vanderzande, A. P. Monkman, B. Champagne and W. Maes, *Dyes and Pigments*, 2021, 186, 109022.
- [145] T. Cardeynaels, S. Paredis, A. Danos, A. Harrison, J. Deckers, S. Brebels, L. Lutsen, D. Vanderzande, A. P. Monkman, B. Champagne and W. Maes, *Dyes and Pigments*, 2021, 190, 109301.
- [146] T. Cardeynaels, M. K. Etherington, S. Paredis, A. S. Batsanov, J. Deckers, K. Stavrou, D. Vanderzande, A. P. Monkman, B. Champagne and W. Maes, *Manuscript submitted*, 2021.
- [147] M. K. Etherington, N. A. Kukhta, H. F. Higginbotham, A. Danos, A. N. Bismillah, D. R. Graves, P. R. McGonigal, N. Haase, A. Morherr, A. S. Batsanov, C. Pflumm, V. Bhalla, M. R. Bryce and A. P. Monkman, *The Journal of Physical Chemistry C*, 2019, 123, 11109-11117.

Pour vous faire membre de la SRC et accéder gratuitement à la revue Chimie Nouvelle :

il vous suffit de verser au compte BNP Paribas Fortis : BE60 2100 4208 0470
la somme indiquée dans le tableau ci-dessous :

Membres résidant en Belgique et au Luxembourg

Membres effectifs : **50 euros**

- participation gratuite ou à prix réduit à toutes les activités de la SRC
- abonnement gratuit à la revue "Chimie Nouvelle"
- accès gratuit à la bibliothèque de la SRC.

Membres associés : **25 euros**

- réservé, avec les mêmes avantages que les membres effectifs, aux jeunes diplômés du deuxième cycle pendant deux ans, aux professeurs de l'enseignement secondaire et aux retraités.

Membres Juniors : Gratuit

- réservé aux étudiants de dernière année du 2^e cycle universitaire (2^e master), des Ecoles d'Ingénieurs industriels et des graduats en Chimie et Biochimie avec les mêmes avantages que les membres effectifs.

Demandeurs d'emploi : **15 euros**

- mêmes avantages que les membres effectifs + insertion gratuite dans Chimie Nouvelle d'une annonce de demande d'emploi.

Membres résidant à l'étranger

Membres effectifs : **60 euros**

Membres associés : **35 euros**